Biophysical Basis of Thermometry Limitations to Control COVID-19 are Overcome at Transmissive Skin Overlying Brain-eyelid Thermal Tunnels

Marcio Marc Abreu[1,2], Ricardo L. Smith[3], Trevor M. Banack[1], Anna L. Clebone[1], Ala S. Haddadin[1], Tyler J. Silverman[1], Feng Dai[4], David G. Silverman[1,5]†

1. Department of Anesthesiology, Yale University School of Medicine, TMP3, 20 York Street, New Haven, CT 06520, USA

2. Department of Ophthalmology and Visual Science, Yale University School of Medicine, 333 Cedar Street, New Haven, CT 06520, USA

3. Department of Morphology and Genetics, Paulista School of Medicine, Federal University of São Paulo, Rua Botucatu 740, São Paulo, SP 04023-900, Brazil

4. Yale Center for Analytical Sciences, Yale School of Public Health, Yale University, 60 College Street, New Haven, CT 06520, USA

5. John B. Pierce Foundation Laboratory, Yale University, 290 Congress Ave, New Haven, CT 06520, USA

†Correspondence and requests should be addressed to D.G.S. (david.silverman@yale.edu)

Abstract

Essential to management of pandemics, noninvasive thermometry has been hampered by inaccuracies and inconsistencies, due to measurements on low thermal conductivity (*k*) surfaces we show here, which have precluded effective assessment of febrile states for centuries. Discovery of brain-eyelid thermal tunnels (BTT) identified undisturbed thermal transmission from brain. We here report a series of integrated anatomic, histologic, thermal emissive, thermal physiologic and thermometric studies designed to identify, characterize and overcome the biophysical limitations of surface thermometry as currently used worldwide to control COVID-19, which primarily relies on non-contact forehead thermometry. However, forehead has thick and variable dermis (~2000 µm to ~2500 µm) and fat layers (~1100 µm to ~2800 µm) resulting in low-*k* insulation equivalent to wood. During thermal emission, highest skin temperature at forehead, present in only ~3.1% of forehead, averaged 1.07±0.49°C (mean±SD) less than over BTT (p=0.008, two-tailed paired t-test). Thermometric studies (without correction factor) revealed 1.97°C higher temperature at BTT site (BTT°) than forehead. Facial fanning caused 3.5°C reduction in forehead temperature, which do not compromise BTT site, attributable to impact on non-BTT surface sites by variable surface vasculature. Cerebral hemisphere dominance studies uncovered higher BTT° in the dominant side ($P<0.001$ for 0.14°C difference). Like BTT, superior palpebral vein region has thin dermis (~900 µm) and is fat-free, however, BTT has higher intensity light emission due to heat transfer from underlying brain tunnel. Findings bring a new dimension for combating COVID-19 that is aligned with physics and biology, and without any costs whatsoever and undue burden, current worldwide suboptimal low-*k* thermometry can be immediately and conveniently enhanced by brain-enabled thermophysical-based high-*k* signal conversion, which can be implemented by any country, community or individual in the world.

Introduction

We recently reported discovery of bilateral Brain-eyelid Thermal Tunnels (BTT) that transmit thermal signals from the brain via bilateral insulated biological thermal waveguides to high thermal conductivity (*k*) skin overlying the right and left superomedial orbit ($SMOS_{BTT}$) (**Abreu et al., 2020a**). Testing in the context of known brain/core temperature decoupling during neuronal excitation and depression confirmed that a noninvasive sensor placed on the medial eyelid at the $SMOS_{BTT}$ captured the brain thermal signal (BTT°), as evidenced by temperature (°C) difference between BTT° and core temperature (Core°) during the extremes of temperature created by hypothermic cardiopulmonary bypass, seizures, evolving stroke, anesthesia, sedation, sleep, traumatic brain injury, and exercise in a hot climate chamber (**Abreu et al., 2020b**). The correspondence of the surface temperature at the $SMOS_{BTT}$ to internal temperature – without need for a corrective algorithm to account for a thermal barrier – was evidenced by comparison to an intraparenchymal catheter during craniotomy (Abreu et al. 2020a) and an intraventricular catheter after brain trauma (**Abreu et al. 2020b**) and by comparison to internal measures of core (in absence of known brain/core discordance) in patients resting prior to electroconvulsive therapy and minor surgery (**Abreu et al., 2020b**). We attributed the lack of an undisturbed thermal signal at $SMOS_{BTT}$ to its overlying a thermal tunnel without intervening fat-laden dermis or dependence on highly variable surface vessels.

`Here we undertook a series of macroscopic and microscopic assessments applied to thermal emission to determine whether infrared light (referred herein as light) emission at the $SMOS_{BTT}$ is distinguished from emission at neighboring monitoring sites, including those along the distribution of the vessels that form the superior ophthalmic vein (SOV) within the BTT, namely frontal vein, angular vein, and superior palpebral vein (**Abreu et al., 2020a**); and, if so, to identify the macro and micro- thermoanatomic features responsible for distinction(s). If there are prominent distinctions, this would identify a basis for all-too-common failure of surface thermometry to accurately detect fever. Especially if the distinctions vary topographically and temporally, they would identify a major deficiency in traditional surface thermometry. This literally would be of "pandemic magnitude," since fever is a main symptom in COVID-19 (**CDC, 2020)** and countries around the world use surface thermometry as main screening parameter for COVID-19, primarily by non-contact forehead temperature measurement (**Nording, 2020; Normile, 2020**).

According to the Forest Products Laboratory of the U.S. Government, oak has low thermal conductivity, resulting in high insulation that prevents effective heat transfer (**Lewis, 1968; MacLean, 1941; TenWolde et al., 1988**). Notably, tissue thermal conductivity research by the U.S. Army showed that fat tissue has such low thermal conductivity that is equivalent to oak [k = 0.00004 Kcal/(s·N·C)], as disclosed in Textbook of Military Medicine, Table 2.1 (**Wenger, 2002**). Thus, measuring temperature of skin containing fat is equivalent to measuring temperature over a wooden barrier.

Studies here reveal the body's thermophysical barriers and show that fat is the main component of forehead and body surface anatomy, which in aggregate with thick dermis creates a low-*k* wall in the human body that varies greatly across different individuals as well as within the same individual over time. Thus, the main screening method used globally in attempts to detect and prevent COVID-19 spreading relies on a technique to measure body temperature that is equivalent of measuring temperature in a highly insulated surface as if wood. These techniques measuring temperature of skin having such low-*k* greatly compromises, if it does not completely preclude, acquiring clinically useful temperature measurements (particularly epidemiologically

meaningful in large crowd settings), thereby strongly impacting worldwide efforts to manage and prevent COVID-19 spreading. The daunting challenge of asymptomatic COVID-19 transmission (**Arons et al., 2020; Furukawa et al., 2020; Ing et al., 2020**) is thus compounded by worldwide body temperature measurements that unknowingly are not in concert with physics and biology, likely hastening the uncontrolled spread of COVID-19 and the growing death toll occurring throughout the world.

Our findings have prompted us to propose and freely share solutions for what constitutes the primary effort worldwide in the context of the COVID-19 pandemic, that is fever detection. Monitoring at the $SMOS_{BTT}$ with a sensor without the need for a correction factor to overcome impact of compromised transmission would constitute the most effective means of surface monitoring; however, world-wide implementation would not be readily available. Thus, based on the findings herein, we propose brain-enabled thermometry based on the BTT signal that can be immediately implemented to help preserve current thermometry being employed worldwide in attempts to control COVID-19 by detecting febrile states. Considering our morphologic studies that documented alignment of BTT with hypothalamus (**Abreu et al., 2020a**), which is the basis of BTT° specificity for brain (**Abreu et al., 2020b**), we reveal a new thermophysical and brain-based conversion of low-*k* signal to high-*k* BTT°. This allows identifying Brain°-Core° discordance, shown in our studies (**Abreu et al., 2020b**), to detect and manage COVID-19 through characterization of febrile and prefebrile illness, supported by a novel cerebral hemisphere dominance methodology.

We show thermometric limitations in the context of the COVID-19 pandemic and considering the prospect of a second wave (**Ferguson et al., 2020; Moore et al., 2020**) known to be the deadliest (**Johnson & Mueller, 2002; Moore et al., 2020; Tomes, 2010**) urgent measures are warranted to reduce human suffering and save lives. We here provide, not yet recognized, actionable information to optimize screening in ports of entry and a method on how to salvage the suboptimal low-*k* temperature measurements. This is accomplished through herein introduced brain tunnel-enabled signal conversion, without any undue burden and no cost whatsoever, that can be easily and immediately implemented, by any country, community, school, business, and individual anywhere in the world. And as shown here, neither race nor aging nor gender affects the thermodynamics and light emission from the BTT, allowing thereby the human race in its entirety to benefit from the knowledge and methodologies we disclose here, which opens the path for a biophysical brain-based solution for the ultimate defeat of COVID-19.

Results

We sought to determine the relationships and distinctions of the BTT, peri-orbital anatomy, remainder of the face, neck, and other thermometric sites to characterize the consistency of BTT and its thermophysical features to measure and potentially manage brain temperature and thermodynamics. This was achieved with a series of integrated anatomic, histologic, thermal emissive, thermal physiologic and thermometric studies.

Additionally, in light of the greater temperature response of left BTT to bilateral seizures (**Abreu et al., 2020b**), we sought to determine if BTT° is selective for the brain near its internal terminus [shown in our previous anatomic findings to include ipsilateral frontal and temporal lobes and ipsilateral region of peri-hypothalamic triunal system (**Abreu et al, 2020a**)], by quantifying resting BTT° differences ipsilateral to the dominant and nondominant cerebral hemispheres. If there is a distinction according to brain hemisphere dominance, this would provide a breakthrough methodology to delineate brain thermodynamics and consequently the thermal status of the body.

Section 1. Macroscopic, histomorphometric and thermal emissive intersite relationships with $SMOS_{BTT}$ and their implications for low-*k* forehead thermometry

We focused initially on the forehead because of its proximity to the $SMOS_{BTT}$, the frontal vein in the forehead being a tributary of the SOV (**Abreu et al., 2020a**), the presence of a large artery [superficial temporal artery (STA), shown below] and the widespread global attempts to use forehead for body temperature measurement to prevent COVID-19 spreading.

Thermal emission. Colored and gray scale (**Figures 1A,B**) of facial thermal emission with overlying grids for delineating emission topography revealed that the highest light emission (demarcated in red in the gray scale figures) was detected only at the BTT terminus at the eyelid region of the superomedial orbit (SMO) beneath the orbital rim. The second highest emission (demarcated as a green line in gray scale figures) was the halo surrounding the BTT site. This is in sharp contrast to the low and inconsistent thermal emission throughout the forehead and face (**Figures 1A,B**). In five subjects studied with grids overlying thermal emission, the highest skin temperature in sites outside BTT averaged 1.07 (0.49)°C (mean±SD) less than over the BTT (P=0.008, two-tailed paired t-test) and was present in only ~3.1% of the forehead; the remaining 96.9% of forehead (including the region of STA) had temperatures of 1.3°C to 3.6°C below the BTT site (**Table #1**). This is not surprising considering forehead surface having low-*k* as if wood.

	Subject 1 (69 y/o)	Subject 2 (51 y/o)	Subject 3 (28 y/o)	Subject 4 (35 y/o)	Subject 5 (48 y/o)
Site(s) of Highest Temp on Entire Grid:	b1,2-A1,2;B1,2	b1,2-B1	b1;2,B1	c1,B1-2,C1	b1,B1
Sites of Highest Temp on FH (all of which are < BTT):					
>50% of cell		a8,A8,B8	C9		
<50% of cell	E5	d7,A7,C8, B4,C4 C5, F4	a9,F6,A8,A9,A10	a10,G5,C5	e7,e8,a8,a9,A9, B5,B9,F5
Difference (°C) Between Highest Temp on Grid (always at BTT) & Highest on FH, face or neck	0.75	1.04	1.92	0.74	0.88
% of FH With Highest FH Temp (Green Isotherm)	<1%	4.5%	1.5%	2.5%	6.0%
Difference (°C) Between Highest Temp on Grid (always at BTT) & Highest Temp by FH Scan	1.10	1.87	2.72	1.76	1.38

Table #1. Comparative emission via BTT, forehead and other facial sites: Data generated by grid overlying gray scale emission image from face of five subjects (male: 1and 3; female: 2, 4 and 5) to delineate site and temperature: (a) no site had temperature (temp) higher than $SMOS_{BTT}$, (b) sites of highest temperature occurred only at $SMOS_{BTT}$, (c) difference between $SMOS_{BTT}$ and highest temperature outside $SMOS_{BTT}$ ranged from 0.74°C and 1.92°C, (d) only a very small area of forehead (3%) had forehead's highest temperature, and still with an average of 1.07°C below temperature at $SMOS_{BTT}$ (only 4 sites had highest forehead emission in more than 50% of the cell area while 23 sites had highest forehead emission in less than 50% of the cell area), and (e) even scanning of forehead resulted in lower temperature than the $SMOS_{BTT}$ (average of 1.75°C). Figure 1A corresponds to Subject 1 and Figure 1B corresponds to Subject 3.

Despite 41 years age difference (**Figure 1A**: 69 years old, **Figure 1B**: 28 years old) between the two male subjects, right and left BTT of both subjects [shown in color panels as red (Figure 1A) and gray (Figure 1B) are the sites with maximal thermal emission, showing that aging does not measurably impact the light emission from the eyelid at the BTT site. Thus, an intriguing observation surfaced, which we are further exploring in ongoing research. In contrast to other tissues in the body that change emission over time, the blood/fat/skin morphological configuration and the resulting light emission from the eyelid at the brain tunnel is apparently resistant to the aging process. Considering that SARS-CoV-2 infection does not spare any age group, this thermodynamic consistency of BTT further supports BTT° as providing the consistent measurements that are necessary for combating the COVID-19 pandemic as well as to salvage suboptimal measurements in low-*k* skin that is present in the entire body surface, except the upper eyelid at SMOS (and adjacent eyelid, **Section 2**).

Macroscopy applied to thermal emission. Although the forehead skin and its underlying venous system is in direct continuum with the SOV at the external terminus of the BTT (**Abreu et al., 2020a**), as shown here its morphology and thermal emission differs remarkably from the eyelid skin at the $SMOS_{BTT}$. Moreover, despite its prominent vasculature, with a large caliber vessel (the STA) (**Figure 1C**, left panel), the forehead shows low and variable thermal emission (shown in orange and dark red) compared to the highest emission at BTT site, shown in gray color (**Figure 1C**, middle and right panels). Not only the venous system (outside the $SMOS_{BTT}$), but also the arterial system suffers from thermal conductivity and biological impediments due to thermophysical barriers (low-*k* surface) (**Figure 1D**) and biological challenges that results from the highly active and variable forehead arterial vasculature and overall cutaneous blood vessels (**Silverman et al., 1987**). The hampered thermal transmission caused by low-*k* barrier is thereby coupled with inconsistent vasomotor tone that leads to confounding temperature measurements at the forehead (and other low-*k* body surface areas).

Additionally, it is virtually impossible to adjust to changes in vasomotor tone that characterize an artery (e.g., STA) since arteries have large elastic lamina and thick smooth muscle layers. This results in constantly variable blood volume in arteries, and thus variable temperature, which reflects local vascular changes (as elicited by ambient temperature, drugs or even emotions), and not the internal thermal status of the body. Contrarily, the SOV have thin wall and, as a vein, lacks external elastic lamina, which coupled with thin smooth muscle layer, results in virtually no volume variability (**Abreu et al., 2020a**). Thus, there is a consistent volumetric heat capacity that results in consistent fever assessment from the hypothalamic thermoregulatory center, which is essential for effective and early detection of infections by SARS-CoV-2.

Microscopy applied to thermal emission. Comparative histomorphometry and proximate superficial anatomy of the forehead showed thick and variable layers of dermis and palisades of subcutaneous (SC) fat, (shown in left and middle photomicrographs of **Figure 1D**). Forehead skin has low-*k* that is comparable to oak (**Wenger, 2002**) creating thereby a barrier for transmission of thermal energy due to thick layers of insulation. It can be clearly observed in **Figure 1D** that the "invisible" and largely variable thickness (and thus largely variable thermal conductivity) reveals histomorphometrically that forehead (and body surface) thermometry violates laws of physics (by measuring temperature on low-*k* surface equivalent to wood) and biology [by measuring temperature on a largely variable tissue (fat layers) and physiology (constantly changing vasomotor tone)]. Thus, forehead thermometry (and temperature measurements in other low-*k* surface sites) may prevent acquiring useful assessments needed to combat COVID-19, that result in a series of inaccurate results: false negative readings when true fever is present but is not detected as well as false positive readings when fever is falsely detected but the person is truly afebrile (**Section 4**).

In sharp contrast to variable histology outside $SMOS_{BTT}$, the eyelid skin overlying the BTT terminus is fat-free and has consistent thin dermis (**Table #2**) that lacks customary capillary networks (shown in right photomicrograph of **Figure 1D)**, which leads to stable and maximized thermal conductivity at the BTT external terminus. Histomorphometry of BTT surface is consistent across specimens of different subjects (of different races) resulting in uniform high-*k* skin across different individuals (**Abreu et al., 2020a**), which was confirmed in thermal emission studies here showing equivalent light emission from BTT across different races, shown below. Thus, BTT° provides the accurate and consistent temperature measurements across diverse populations, which is necessary to effectively detect the thermal status of the different populations exposed to a disease so widespread globally as COVID-19. Accordingly, the brain-based signal conversion based on BTT° may provide the world with a universal accurate measurement for detecting prefebrile and febrile states across different ethnicities infected with severe acute respiratory syndrome coronavirus 2 (SARS-CoV-2) around the world.

Table #2. Comparative histomorphometry of skin of BTT site and other regions:
Thickness (in microns) of the Epidermis, Dermis and Fat layers. The two BTT skin specimens were the only ones with the similar dermis thickness and no SC fat (further corroborating our previous histologic study of eyelid skin at the BTT site, **Abreu et al., 2020a**). In contrast, forehead skin from different cadavers have substantially different thickness of epidermis, dermis and fat layers. Thick dermis and fat layers observed from neck and axilla (**Section 2**) follow the same pattern of forehead; with variable thickness among cadavers.

Tissue	BTT(1)	BTT(2)	Forehead(1)	Forehead(2)	Neck	Axilla
Epidermis	~70	~70	~70	~100	~70	~100
Dermis	~900	~900	~2000	~2500	~2500	~2000-3000
Fat	0	0	~2800	~1100	~2200	~3000-8000

Radiant emission from $SMOS_{BTT}$ is consistently located in the eyelid, that is coupled with consistent BTT skin microscopy (**Table #2**) and aligned with previously shown constant histology (**Abreu et al., 2020a**), which is also associated with consistent vein anatomy (**Bergen, 1981; Cheung & McNab, 2003; Festal, 1887**). This results in remarkably consistent biology, comprised of a combination of constant macroscopic and microscopic features only occurring at the BTT site. This provides uniform brain↔surface thermal physics that optimize intensity and consistency of light emission from BTT. In sharp contrast, the presence of fat and thick dermis in the forehead (and areas outside the $SMOS_{BTT}$) (**Table #2**) have led to the inclusion of correction algorithms and factors in forehead thermometry resulting in further hindering the ability to correctly measure temperature because of the large variability of fat and dermis in different individuals, and over time in the same individual, which is also found in other surface regions throughout the body.

Measurements at the BTT site enables unique thermal transmission, that results in accurate and precise temperature measurements that are not influenced by ambient temperature or vasomotor tone since the tunnel is shielded inside the orbit and the vein lacks external elastic lamina thereby preventing any meaningful changes in volume. In contrast, the superficial temporal artery (**Figure 1C**) and other facial vessels (**Section 2**) course parallel to the skin surface and thus are vulnerable to changes in ambient temperature; and their elastic wall makes their caliber prone to changes, not only due to environmental temperature but also to emotional state, leading to forehead temperature measurements to provide unreliable and inconsistent readings.

Notably, another distinction that enables unique, accurate and precise brain thermometry at the BTT site (and the use of the signal conversion proposed here) is the lack of an artery accompanying the vein (SOV) of the tunnel (**Abreu et al., 2020a**). Contrarily, the vascular system on body surface is centered on the presence of an artery-vein configuration. For example, another site used for temperature measurement, the wrist, consists of radial vein, which are paired vein that accompany the radial artery through the back of the hand and the lateral aspect of the forearm. Thus, wrist measurements, besides having low-*k* surface suffer from the impact countercurrent heat exchange. Additionally, the wrist is exposed to the environment, thus wrist measurements may simply reflect the ambient temperature [cold environment causing cold wrist skin and underestimation that may lead to false negative reading (and failure to detect fever), and warm environment causing warm wrist skin and overestimation that may lead to false positive reading (and falsely detect fever)]. Furthermore, wrist measurement suffers from the drawbacks of the presence of an artery, which is characterized by internal and external elastic lamina and variable vasomotor tone, which further impacts temperature measurement.

The numerator of heat dissipation equation (and thus thermal transmission) is largely dependent on *k* and denominator on thickness. Since dermis and fat have low *k* values, lack of fat and minimal dermal thickness maximizes thermal conductivity of skin (**Table #2**). We showed previously (**Abreu et al., 2020a**) that the skin overlying the BTT terminus is fat-free and has the thinnest dermis resulting in unique radiant high-*k* skin, which was further confirmed by the morphologic and emissive studies shown here. This makes the $SMOS_{BTT}$ the optimal site for temperature measurement on the body surface.

The BTT has one unique and highly radiant surface corresponding to the underlying anterior orbital portion of the tunnel in the right and left eyelid and a single beam of light is generated at each BTT site (**Figures 1A-C)**. The unique thermally transmissive and emissive brain tunnel thermodynamics and architecture allow a BTT sensor to consistently and continuously measure brain temperature and to provide the most accurate body temperature measurement individually and across populations, as shown here and by previous studies (**Abreu et al., 2020b**).

Brain thermodynamics of BTT provides the basis for the brain conversion signal for salvaging low-*k* thermometry currently used around the world [including usage in epidemiologically high risk large crowd settings such as military bases and large entertainment venues (**Section 5**)], which is sorely necessary for controlling the unimpeded spread of COVID-19, as currently occurring.

Figure 1. Macroscopic, histomorphometric and thermal emissive relationships of SMOS$_{BTT}$ with low-*k* forehead surface. Bar represents grades of infrared light emission from highest (gray) to lowest (brown-black). Temperature levels are provided in Table #1 and in text. (**A,B**) Comparative facial thermal images of 2 normal resting subjects [(69 years old (Figure A) and 28 years old (Figure B)]; color and gray scale with overlying grid to delineate thermal map and sites of maximal light emission. Grid identified right and left BTT as the only sites of maximal light emission in both subjects, documenting inability of forehead thermometry to provide useful measurements to control COVID-19, in both mature and young populations.

Figure 1A

Macroscopic, Histomorphometric, and Thermal Emissive Relationships of Forehead

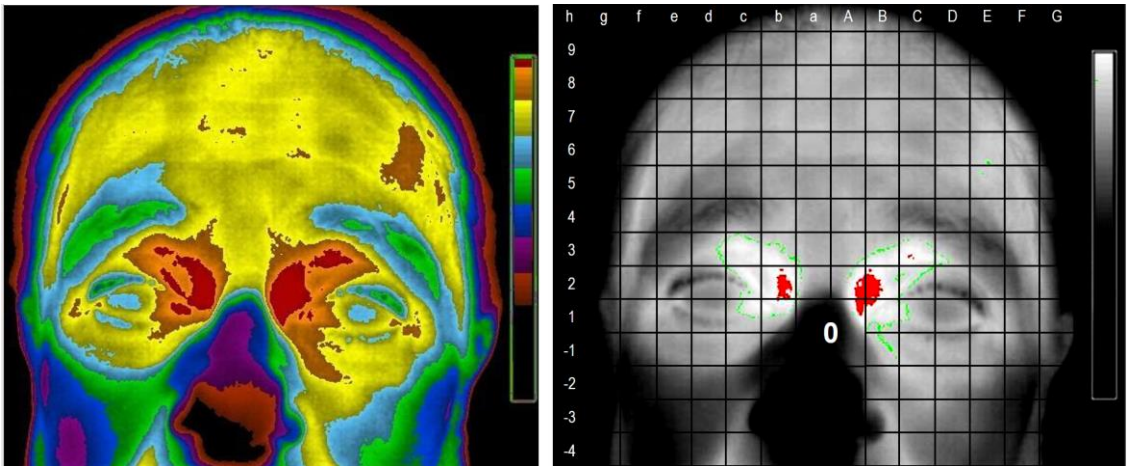

(**A**) BTT = highest thermal emission [(red color) and (b1,2-A1,2;B1,2 in map of Table #1)]. Forehead (and STA region) have lower temperature and variable thermal emission (yellow color). Only one small area remote from BTT (red) and halo (<1.5 mm diameter corresponding to E6 on grid) had emission equivalent to halo, but not equivalent to BTT.

Figure 1B

Macroscopic, Histomorphometric, and Thermal Emissive Relationships of Forehead

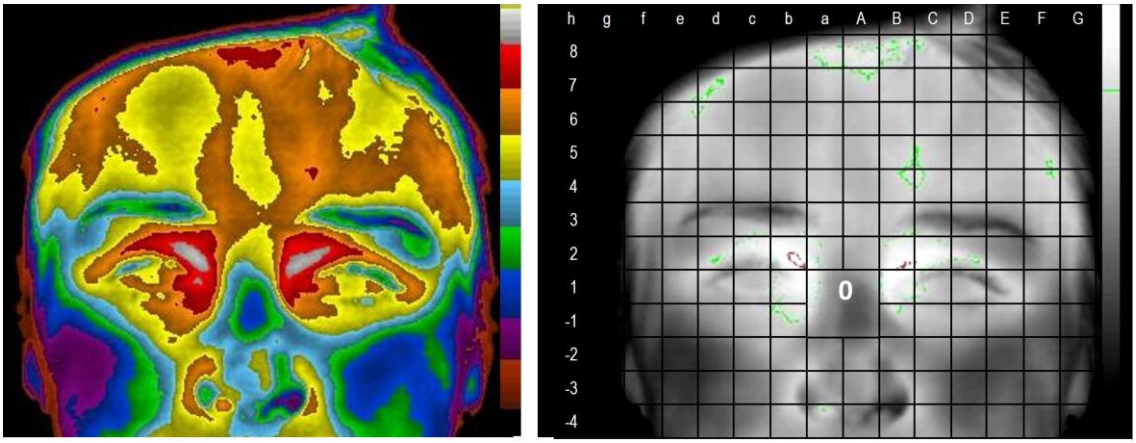

(**B**) BTT is the site with highest thermal emission, shown in gray (b1,2;B1 in thermal map, Table #1). Forehead has low emission (yellow-orange) and few areas of green isotherm in less than 3% of the area (Table #1).

Figure 1C

Macroscopic, Histomorphometric, and Thermal Emissive Relationships of Forehead

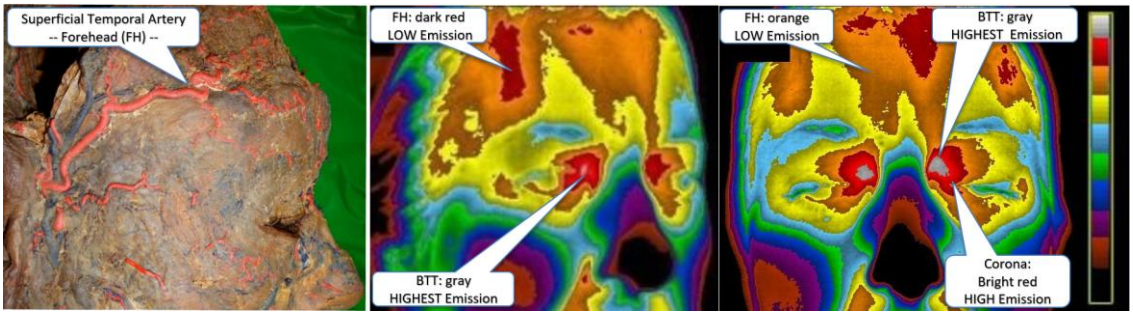

(**C**) Comparative forehead vasculature and thermal emission. *Left*: Formalinized head showing STA infused with red Neoprene. *Middle:* Thermal emission from side of face to show STA region, showing low thermal emission (orange and dark red) in contrast to highest emission at BTT site (gray) and its halo (bright red). *Right*: Frontal facial light emission showing BTT at the upper medial eyelid as the area of highest light intensity; second highest emission at the halo, while forehead (orange and dark red) and all other facial areas show lower intensity.

Figure 1D

Macroscopic, Histomorphometric, and Thermal Emissive Relationships of Forehead

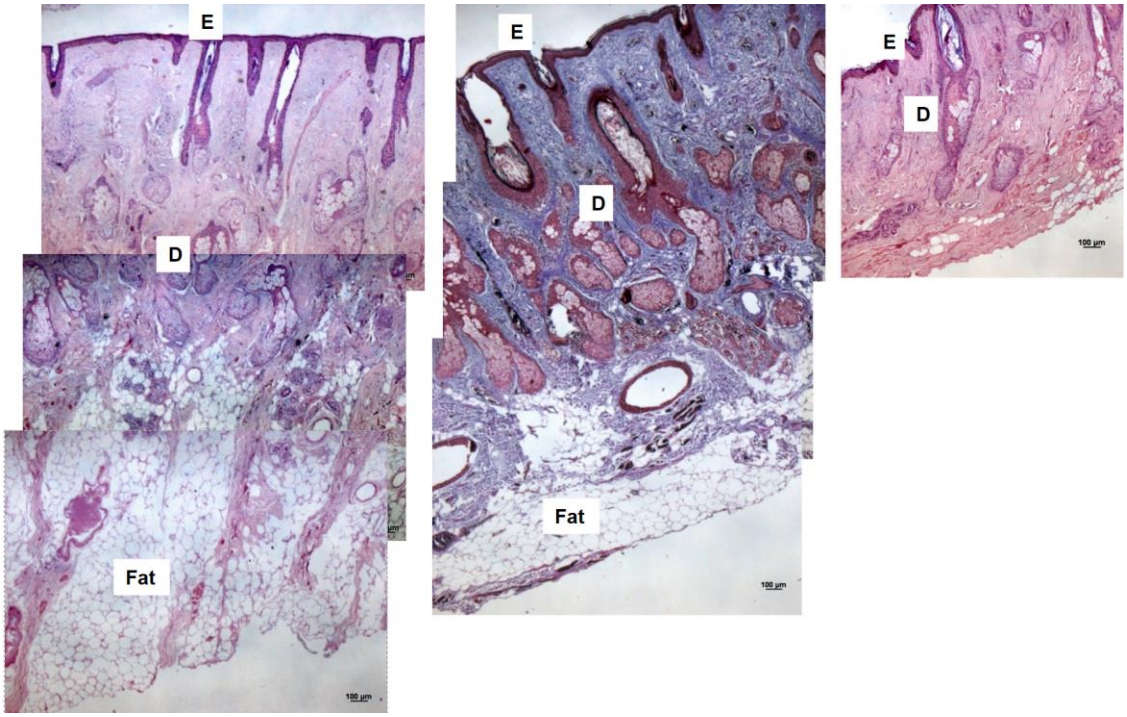

(D) Photomicrographs contrasting skin specimens from forehead and skin overlying the BTT. E = epidermis, D = Dermis. Dimensions given in Table #2. *Left*: Forehead skin has a variable and thick dermis, and layers of SC fat. Combined thickness of SC fat and dermis is so broad that a *3-slide composite* was required to show all layers in one single image. *Middle:* Markedly different thickness and histologic structure in specimen from the same forehead region, but from a second cadaver specimen, revealing flat thick layer of fat measuring one third of specimen on left (Table #2). *Right*: In sharp contrast, BTT skin specimen has thinnest D and absence of SC fat allowing inclusion of all layers in *one single slide.* As reported (**Abreu et al., 2020a**), all specimens of $SMOS_{BTT}$ have equivalent thickness and structure despite different races.

Section 2. Macroscopic, histomorphometric and thermal emissive relationships with $SMOS_{BTT}$ and their implications for additional low-*k* surface thermometry

We focused on areas of veins adjacent to $SMOS_{BTT}$ and anatomic surface regions relevant to thermometry. The BTT terminus in the medial eyelid is the point of convergence of three veins [frontal vein (FV) shown in **Section1**, superior palpebral vein (SPV), and angular vein (AV) (**Abreu et al., 2020a**)]. Notably, all 3 vessels have consistently lower emission in relation to the BTT shown as a central highly emissive hole depicted with surrounding red halo of lower emission (**Abreu et al., 2020a**). However, the SPV shows a particular and unique pattern of high intensity thermal emission that declines with increasing distance from the medial eyelid at the BTT.

Superior palpebral vein region. To further characterize the region adjacent to the $SMOS_{BTT}$ and understand from a morphologic standpoint the basis for the unique radiant emission along the SPV we dissected the SPV region adjacent to where it joins the BTT site and performed histomorphometric analysis of the specimen. Remarkably, the SPV skin region is void of fat, and has similar structure and dimension as the eyelid skin of $SMOS_{BTT}$: skin thickness is equivalent to the BTT skin, and both anatomic regions (SPV and BTT) do not have fat layer (**Figure 2A**). This finding irrefutably corroborates that, without an underlying tunnel, thermal emission on the body surface (beyond eyelid region of the $SMOS_{BTT}$) even if with minimal fat layer, cannot correspond to the internal (brain or core) thermal status of the human body including all surface body sites currently being used for screening COVID-19 worldwide. Decline of SPV emission with increasing distance from the BTT site further indicates lack of an underlying thermal path from the middle cranial fossa (MCF) akin to MCF↔SMOS transorbital thermal tunnel (**Abreu et al., 2020a**).

Whereas the distinction between highly vascularized facial sites (including the forehead) and the BTT site at the medial upper eyelid is attributable largely to the consistently thin and fat-free high-*k* skin of the $SMOS_{BTT}$ (**Figure 1D**), the essential and indispensable feature for the unique light emission identified and having minimal intersubject variability is the presence of the underlying tunnel communicating with the brain. This unique thermally transmissive brain tunnel structure further confirms that a BTT sensor acquires undisturbed brain thermal energy and provides the most accurate temperature measurement (**Abreu et al., 2020b**)

Angular vein region. Likewise, despite having a rich and large vascular network (**Figure 2B,** left panel) which includes large caliber vessels (angular vein and artery), the malar region has low thermal emission (shown in orange-yellow-blue in middle panel as opposed to highest intensity shown in gray at BTT) , attributable to low-*k* histology (thick dermis and fat layers, shown in right panel) and lack of an underlying tunnel (**Abreu et al., 2020a**).

Neck. Despite having major vessels such as jugular vein and internal carotid artery [which communicates with the BTT via the triunal system (**Abreu et al., 2020**)], neck also has low thermal emission (**Figure 2C**, left panel) and low-*k* histology (**Table #2**) and no underlying tunnel. Hence, the neck (like malar and forehead region) despite having large caliber vessels failed to achieve thermal emission comparable to the eyelid at the $SMOS_{BTT}$.

An irrefutable thermal emissive evidence of the inability of forehead measurements to accurately detect infection and prevent spread of COVID-19 is disclosed exemplarily in thermal emission, as seen in **Figure 2C** (51 years old, female). As clearly seen, the forehead is very cold **(**blue and green) and has a temperature approximately 3.0°C lower than BTT (shown in gray). Low thermal emission observed reflects temperature of a *local* cold tissue as opposed to the true *internal* warm status of the body shown at the BTT site. If forehead measurements were taken (as shown below), they would deceptively indicate normothermia (or hypothermia) and would fail to detect fever in infected populations with SARS-CoV-2, both at the individual level or during mass screening at airports and ports of entry. These false negative readings may lead to virus spreading, besides increased morbidity and mortality due to delay seeking care. Despite correction factors, these surface sites, outside the BTT, may fail to provide thermal emission (and temperature measurements) that detect the presence of fever, as evidence by even 3°C difference between the true thermal status of the body and forehead temperature.

Axilla. Another skin site frequently used for temperature measurements, the axilla, illustrates the combined low-*k* barriers that cover the body surface. In contrast to skin at $SMOS_{BTT}$ that has the thinnest dermis (**Table #2**), the axilla and remaining of the body surface is

characterized by the presence of fat and thick dermis. [except SPV region (**Figure 2A**)]. This can be exemplarily observed in the axilla specimen of two corpses (**Figure 2D**), which shows a large low-*k* barrier comprised of thick dermis and fat. Macroscopically, dermis is seen as a thick white band between epidermis and fat. Due to its thickness, histologically, dermis encompasses the majority of the slide. Axillary temperature measurements as well as thermometry in other body surfaces (e.g., wrist, arm, back of the head, and face) have similar impediments, due to low-*k* barrier, as the forehead, leading to false positive and negative readings, illustrated below, for the forehead (**Section 4)**. Thermophysical barriers that create a thermal wall in the human body have turned into barriers that preclude effectively combating COVID-19, since measurements in any skin surface (outside $SMOS_{BTT}$) encounters a combination of low-*k* tissues (with high variability of thickness and structure among different subjects) that prevents clinically useful readings necessary in the context of a pandemic.

Figure 2. Macroscopic, histomorphometric and thermal emissive relationships of $SMOS_{BTT}$ with low-*k* body surfaces. Bar represents grades of infrared light emission from highest (gray) to lowest (brown-black). Temperature levels are provided in text. Comparative images of macroscopy, microscopy and thermal emission of areas adjacent to BTT and low-*k* surface used for thermometry.

Figure 2A

Macroscopic, Microscopic and Thermal Emissive Relationships with Low-k Surfaces

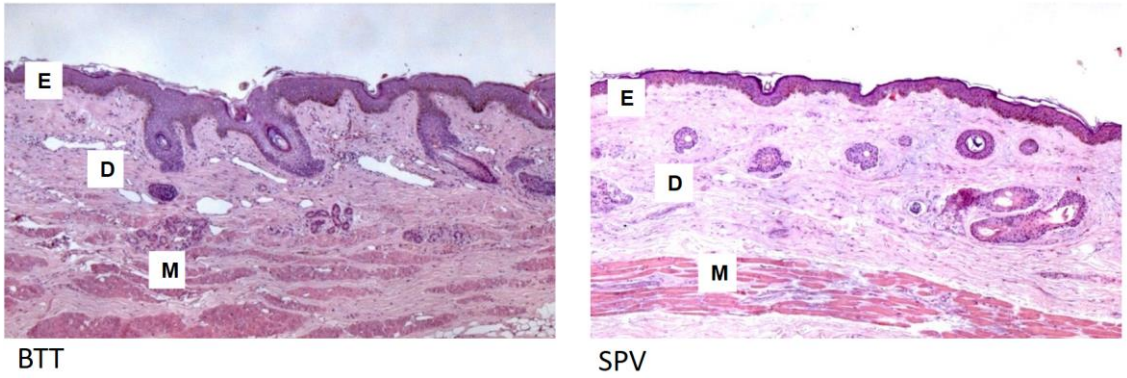

(**A**) Comparative skin histology of SPV region and BTT showing similar skin histomorphometry of BTT (left) and SPV (right). Both skin specimens have thin D and absence of SC fat (900 microns). Orbicularis muscle (left) and tarsal muscle (right) are seen below the dermis revealing unique morphology in the body, where dermis rests directly on muscle.

Figure 2B

Macroscopic, Microscopic and Thermal Emissive Relationships with Low-k Surfaces

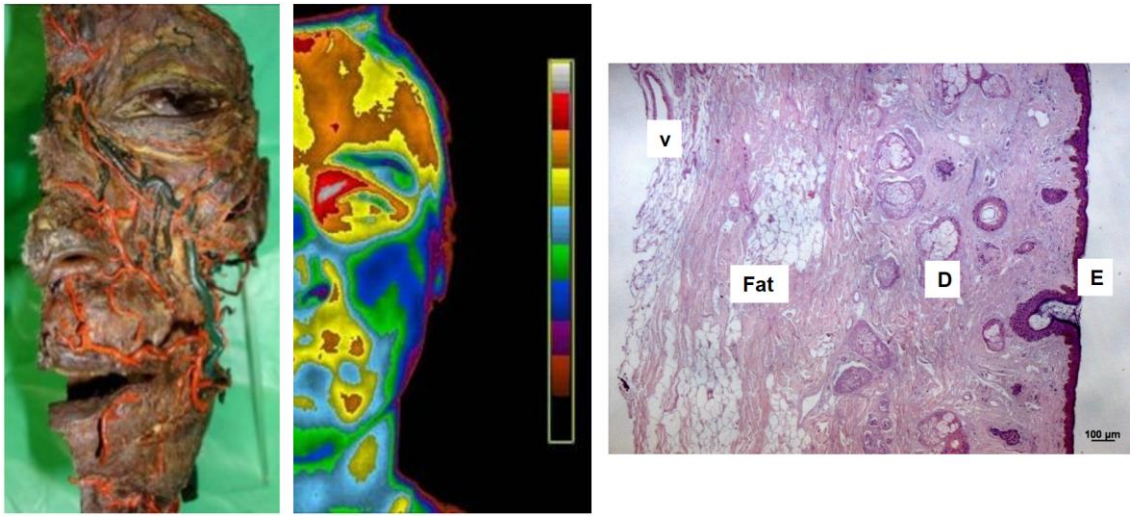

(**B**) Comparative vasculature, thermal emission, and histology of malar region (angular vein). *Left*: Formalinized hemiface (injected with red neoprene in arterial and blue in venous system) showing vast and large caliber arterial and venous facial network. *Middle:* Thermal emission from the hemiface (28 years old, male), showing lower temperature throughout the face and forehead (blue-green-yellow) than at the BTT site (gray). *Right*: Photomicrograph of malar region showing thick dermis and layers of SC fat with blood vessel (V) beneath the fat layer, aligning histology of thick skin and fat with low thermal emission, despite large caliber vessels.

Figure 2C

Macroscopic, Microscopic and Thermal Emissive Relationships with Low-k Surfaces

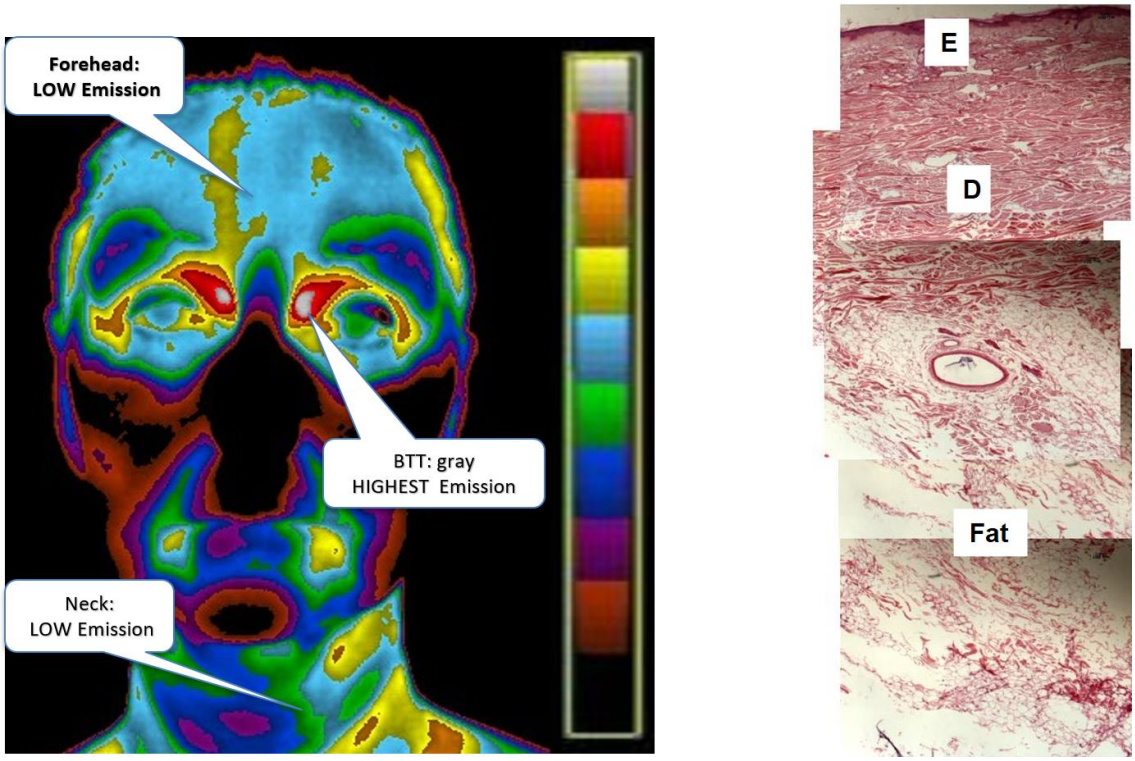

(**C**) Comparative thermal emission and neck histology. *Left*: Facial thermal emission shows low emission from neck despite large jugular vein and carotid artery. Note very cold forehead (shown in blue-green), in sharp contrast to high intensity eyelid emission at BTT (horn configuration) with gray center of maximum intensity surrounded by lower intensity zone in red color. *Right*: Photomicrograph showing thick dermis and large fat layer creating a low-*k* barrier in the neck (Table #2).

Figure 2D

Macroscopic, Microscopic and Thermal Emissive Relationships with Low-k Surfaces

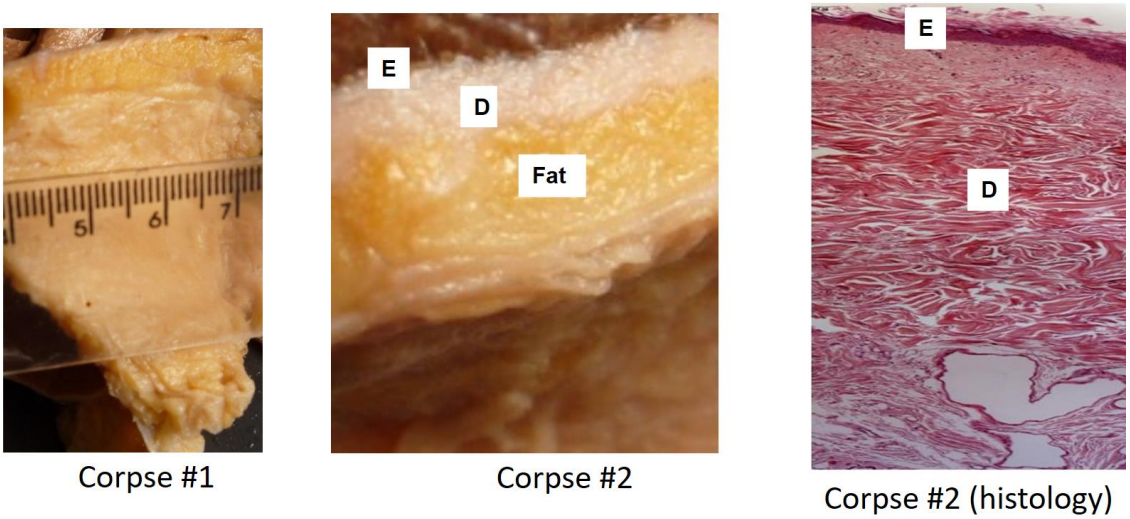

(D) Axilla: gross sections from two corpses (left and middle panels) showing thick dermis, and great variability in thickness of dermis and fat (Table #2). Adipose tissue measures from 3 mm in some regions up to 8 mm in the specimen shown here (a lot of fat remains in the armpit of the corpses, between blood vessels, nerves and lymphatics). Right panel is photomicrograph showing histology of the region of corpse #2: dermis (2500 µm) corresponding to the white area in gross section.

Section 3. Resting and dynamic thermal transmission at BTT, Core and Periocular Sites

To irrefutably corroborate that, without an underlying tunnel, thermal emission on the body surface (beyond eyelid region of the $SMOS_{BTT}$) cannot correspond to the internal (brain or core) thermal status of the human body, we performed additional resting and dynamic assessments of thermal transmission via BTT, oral mucosa (representing core temperature) and periocular skin (i.e., SPV) and mucosal (i.e., caruncle) sites.

As seen in **Figure 3A** neither SPV or caruncle (inner canthi) has emission equivalent to the highest isotherm, shown in red at the $SMOS_{BTT}$, in which emission from BTT and oral mucosa have the highest intensity. This finding further supports that heat transfer from superficial mucosal vessels (not from internal blood vessel as the SOV) reflect local mucosa temperature (as for the caruncle). Temperature of such mucosal surface is greatly influenced by humidity, wind, and even simple inflammatory process in the eye such as conjunctivitis. Thus, measurements of inner canthi (such as by thermal imaging) in screening for COVID-19 may deceptively overestimate temperature, due to emission resulting from a local infection, or underestimate by reducing blood flow as occurring during vasoconstriction and changes in humidity. Moreover, use of eye drops that alter vascularity may generate inconsistent heat transmission, since conjunctival vessels and caruncle are characterized by highly reactive vascular response. Thus, quantifying emission from

inner canthi is suboptimal in many situations, let alone not having a connection with the brain or ability to detect early thermal changes (**Abreu et al., 2020a**) as provided by thermal measurements at the eyelid in the BTT site (**Abreu et al., 2020b**). As shown in **Figure 3A,** the caruncle (inner canthi, shown as green isotherm) has much lower thermal emission than the BTT site (shown in red). These biological and thermophysical impairments found in the inner canthi resulted, as expected, in failing to detect infected individuals during mass screening (**Priest et al., 2011**), and such suboptimal screening techniques may not be sufficient to contain a virus highly transmissible as causing COVID-19.

We also assessed the impact of a body core thermal challenge on BTT thermal emission, consisting of hand and forearm immersion in ice water (**Figure 3B)** with simultaneous assessment of thermal emission from core (oral) and from surface (skin), which showed that $SMOS_{BTT}$ emission was uniquely maintained during cold immersion, a challenge that caused emission from other facial regions (including nearby SPV skin, caruncle and oral mucosa) to decline, revealing a key distinction not only between $SMOS_{BTT}$ and neighboring skin, but also between $SMOS_{BTT}$ and core temperature (oral mucosa).

The low thermal emission detected from forehead and other body surface areas, shown above, results from a combination of low-k tissues (fat and dermis). Although fat has the lowest thermal conductivity [k = 0.00004 Kcal/(s·N·C)], dermis, likewise, is characterized by high insulatory properties [k = 0.00009 Kcal/(s·N·C)]. In contrast to skin at $SMOS_{BTT}$ that has the thinnest dermis (**Table #2**), the remaining of the body surface [except superior palpebral region (**Figure 2A**)] is characterized by the presence of fat and thick dermis (including sites used for measurement such as wrist, arm, and chest) have similar impediments, due to low-k barrier, as the forehead, leading to false positive and negative readings, illustrated below, numerically for the forehead (**Figures 4B,C**).

Figure 3. Resting and dynamic thermal transmission at BTT, Core and Periocular Sites

Bar represents grades of infrared light emission from highest (white) to lowest (black). Temperature levels are provided in Table #1 and in text. Comparative facial thermal images at rest and during immersion in ice water to show distinctions of emissions from BTT, oral mucosa, ocular mucosa (inner canthi, caruncle) and skin surface (SPV and forehead), which identified right and left BTT as the sites of maximal light emission. in both, at rest and during cold challenge.

Figure 3A

Resting and Dynamic Thermal transmission at BTT, Core and Periocular Sites

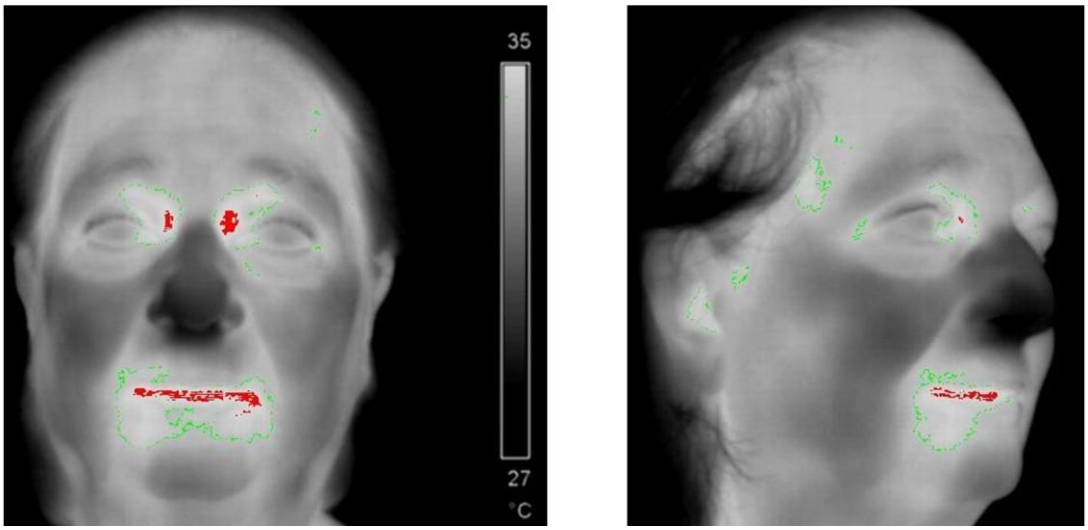

(**A**) Gray scale facial thermal emission (subject in Figure 1A). *Left*: Oral cavity reflects core temperature and shows similar emission as BTT (both sites having red isotherm surrounded by green isotherm). Right and left BTT have highest surface emission. Outside BTT and oral, emissions vary greatly in intensity and location. *Right*: side view shows lack of high emission at the caruncle and SPV [green isotherm (but no red) shows lack of high thermal emission as BTT].

Figure 3B

Resting and Dynamic Thermal transmission at BTT, Core and Periocular Sites

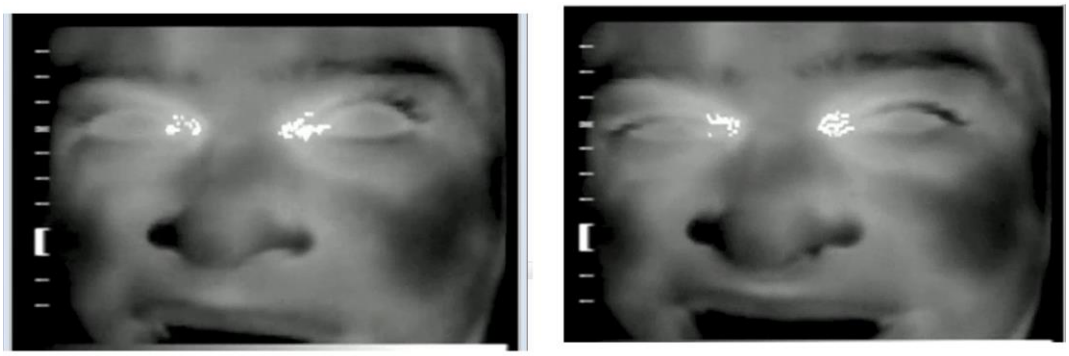

(**B**) Initial frame (left) and last frame (right) of video of experiment (upper arm immersion in ice water). At baseline, similar emission from caruncle and BTT site. During immersion, forehead, palpebral, nasal and cheek regions have a darker hue, and caruncle emission decreases while BTT site remained virtually unchanged from baseline, with same bright light emission. Oral cavity (black) has much lower emission than BTT; this suggests cooling of core but not of BTT (brain temperature), as shown in previous studies (Abreu et al., 2020b).

Section 4. Quantification and models of intersite distinctions for BTT, core and forehead

In all subjects tested, sites outside BTT terminus (including forehead) were "silent" for high thermal emission as compared to light emission from $SMOS_{BTT}$, further evidenced in **Movies #1 to #3 (Supplemental Information).** As documented in our real time infrared light emission a single beam of light is generated at each BTT site, represented by an essentially circular gray image of high emissivity in the photograph, and in pixels of red color in said movies. The above findings provide thermophysical confirmation that intraorbital blood/fat tunnel configuration and external high-*k* skin surface [(**Abreu et al., 2020a**) and (**Figure 1D**)] provide the thermodynamics for emission of two light beams of high intensity, in each of the eyelids (right and left), as shown herein (**Figures 1A-C, 2C,3A,B**), which are thermo-physically connected with the brain thermoregulatory center (**Abreu et al., 2020a**). However, none of the other facial and body regions achieve the emission of high intensity beams that are present in the BTT, as clearly observed.

Quantification. In order to more effectively quantify intersite distinctions (and hence fever detection) identified by thermal imaging and thermometry, we assessed 80 data points that had been acquired in 18 volunteers sitting in a temperature-regulated room (mean temperature 22°C). Each subject was tested once daily for 2 to 5 successive days at the $SMOS_{BTT}$ and sites of core (sublingual, SL) and surface measurement (forehead). BTT° was recorded as the highest temperature obtained with a handheld sensor with no correction factor (Abreu BTT C-1 Probe, BTT Corp, Aventura, FL) positioned over the $SMOS_{BTT}$ for 10 seconds. Forehead temperature (FH°) was assessed with same handheld sensor, capturing the highest temperature upon positioning over the ipsilateral forehead for 10 seconds. Body core temperature was measured by sublingual (SL): SLraw° via a thermometric catheter under tongue for 3 minutes; and SLdigital° via digital thermometer with corrective algorithm for 5 seconds. These sites and devices generated the following values (mean±SD): BTT° 36.22(0.4)°C; FHº 34.25(0.8)°C; SLraw° 36.15(0.5)°C; and SLdigital° 36.38(0.5)°C. The measured 1.97°C higher temperature at the BTT site than the forehead location is consistent with thermal emissive investigations (**Table #1**).

The high variability at the forehead (beyond the BTT and its halo) was evidenced by the highest standard deviation (±0.8°C) of FH° among the different thermal sensors at the 80 data points. This is consistent with the variation among sites and subjects in **Table #1**. Large variation of forehead temperature (3.4°C) is attributable to varying thickness of forehead fat and dermis within and among individuals (**Table #2**). Even at its most transmissive point, forehead temperature was below that of the BTT and oral mucosa (core). Unless corrected, forehead thermometry for individual patients as well as forehead thermal imaging for mass screening will repeatedly lead to underestimation. However, even if adding correction or fudge factors, measurements that violate thermal physics and biology by measuring a low-*k* surface with variable thickness and changing vasomotor tone cannot prevent underestimation, as shown illustratively in subject of **Figure 2C**, who has very low forehead temperature, leading to failure to detect infection and spread of COVID-19. Likewise, overestimation may occur, exemplified by using the same artificial correction factor for subject of **Figure 2C** in a subject with forehead temperature approximately 1.5°C higher, as seen in subject of **Figure 1B**. This forehead measurement results in an individual having true temperature of 37°C to be falsely diagnosed with a temperature of 38.5°C, leading to false diagnosis of fever and placement of normal population in quarantine with infected populations, which besides causing injury to a healthy individual causes spread of COVID-19.

As noted above, inclusion of a correction factor can confound assessments (individual and mass screening) since the same correction factor applied to a device to correct for interference of

the temperature recording by the body's thermal barrier introduces error if the factor is either too high or too low for a given patient in accordance with the wide range of intersite differences shown in **Table #2** and **Figures 1A-C, 2C,3A,B**). Moreover, the correction factor itself could be erroneous for the overall population. It has been shown that the mean value for normothermia in the 21st century is 36.67°C (**Protsiv et al., 2020**), which is less than the historical value of 37°C. Usual artificial correction to 37°C as mean for normothermic subjects thus would lead to a spuriously high value. In the 80 time-point sample, SLdigital° (with correction factor) exceeded SLraw° by 0.24(0.5)°C, leading individuals having true temperature of less than 38°C to fall into a level of fever which, based on US Government guidelines, is consistent with levels present during infection by SARS-CoV-2 (**CDC, 2017; CDC, 2020**).

Models. We combined our histomorphometry findings with our thermal emissive findings to illustratively document numerically the large negative impact on the COVID-19 pandemic due to assessing thermal status of the body through measuring temperature of a surface with low-*k*, as present in the forehead (and other skin surface, except BTT skin overlying the tunnel). Currently, attempts to control the pandemic and detect infection worldwide, primarily relies on measuring temperature of a low-*k* surface, and in the case of the forehead (**Figures 1B,2C**) the equivalent to measuring temperature of various types of wood due to great variability in the amount and thickness of fat layers as observed in our histology specimens (**Figure 1D**), which was confirmed by the large variability of thermal emissions (**Figure 1B**). False negative readings leading to spreading COVID-19 results from thick fat layers that generates low thermal emission (**Figure 2C**). This causes the true temperature of 38.2°C to be underestimated and read as 37.0°C by forehead thermometry (despite using artificial correction factor of 1.0°C that is added to measured value of 36.0°C), in contrast to BTT that has no fat and no need for correction factor, thus capturing the true thermal status of the body, and detecting infection (thereby preventing virus spread) (**Figure 4B**). Likewise, false positive readings leading to unnecessary quarantine, and placing healthy individuals with infected ones (further spreading COVID-19) results from thin fat layers, shown representatively as a thin and flat slab, that generates relatively higher thermal emission (**Figure 1B**). This causes the true temperature of 37.3°C to be overestimated and read as 38.1°C by forehead thermometry (due to an artificial correction factor of 1.0°C that is added to measured FH value of 37.1°C), in contrast to BTT that has no fat and no need for correction factor, thus capturing the true thermal status of the body, and not detecting false fever, thereby preventing COVID-19 spread by avoiding healthy population being isolated with infected ones (**Figure 4C**).

Figure 4. Quantification and models of intersite distinctions for BTT, core and forehead.

Figure 4A

Quantification and Models of Intersite Distinctions for BTT, Core and Forehead

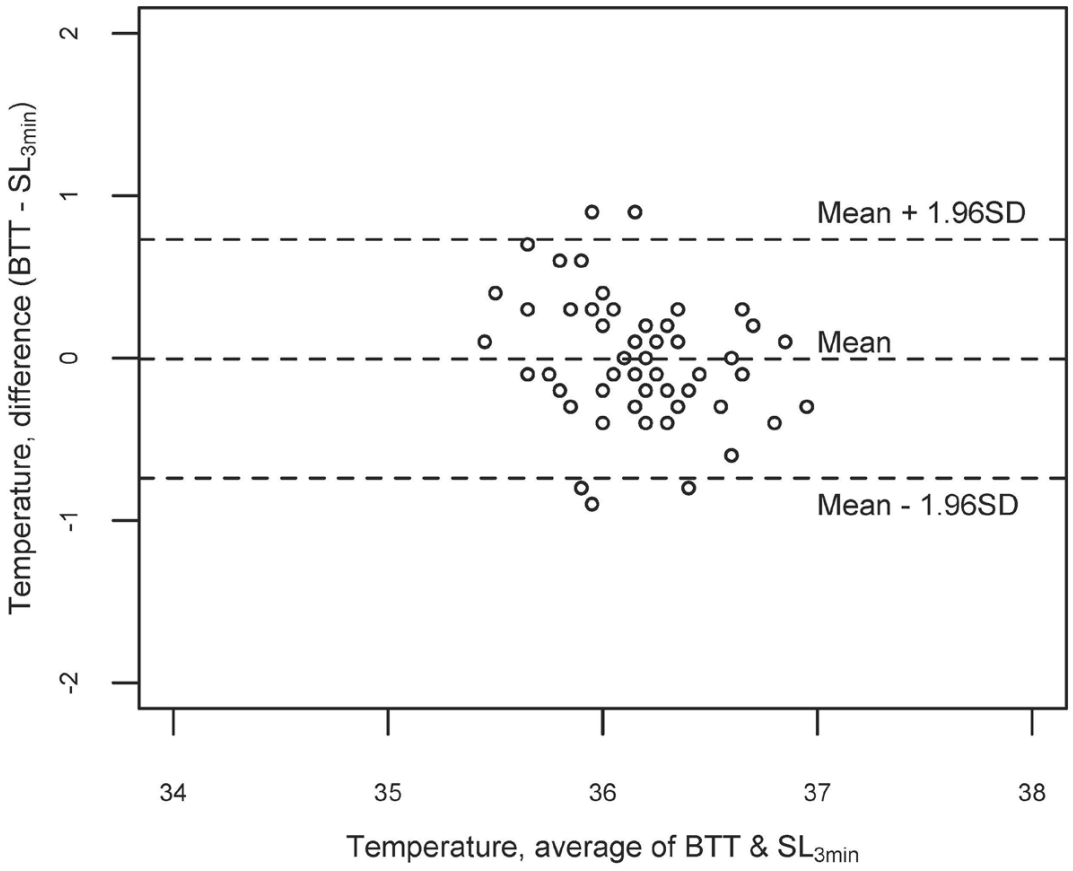

(**A**) Bland Altman display (80 data points) of BTT° (obtained with hand-held sensor) and SL° (obtained with thermistor under tongue for 3 min) in 18 healthy volunteers under resting conditions on up to five different days; mean±SD = 0.073±0.6°C.

Figure 4B

Quantification and Models of Intersite Distinctions for BTT, Core and Forehead

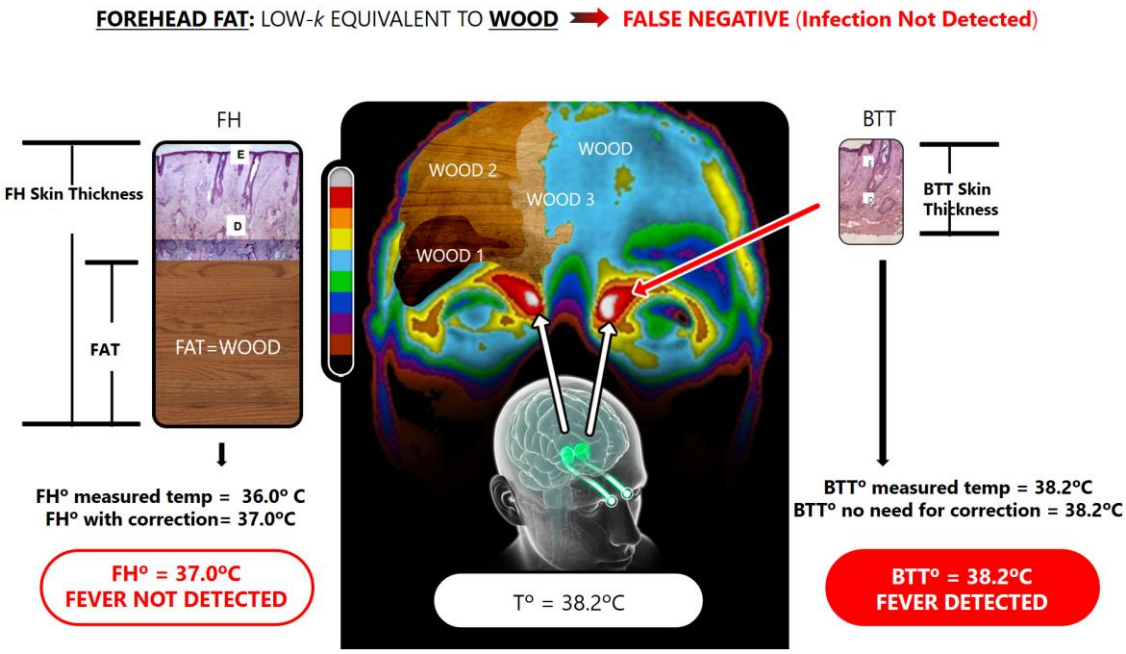

(**B.C**) Central panel shows colored thermal image of BTT at the eyelid, forehead and periocular regions (upper image) and in the lower image an illustration of the bilateral brain-eyelid thermal tunnels (with hypothalamic region at the center of the brain in green). Thermal image of forehead shows variable low-*k* (1,2,3) representing different thermal emission zones on FH. BTT site in thermal image is illustratively connected to the source of infrared light in the brain (hypothalamus) at the internal terminus. Right panel shows specimen of BTT skin characterized by fat-free histology, with red arrow pointing to the external terminus of the BTT as the area of highest thermal emission in the image. White arrow illustrates the connection of the center of the brain with the fat-free histology region at the external terminus of the BTT. Numerical values illustrate: a) left panel (measurement at forehead with current thermometers using correction factor), b) right panel (measurement at BTT without a correction factor), and c) middle panel: brain temperature.

(**B**) Left panel shows thick wood representing thick fat layer in histological specimen, which results in very low forehead temperature. Comparative thickness between BTT skin and FH skin can be observed -- thick fat layer results in underestimation of true temperature leading to false negative reading (see text for details).

Figure 4C

Quantification and Models of Intersite Distinctions for BTT, Core and Forehead

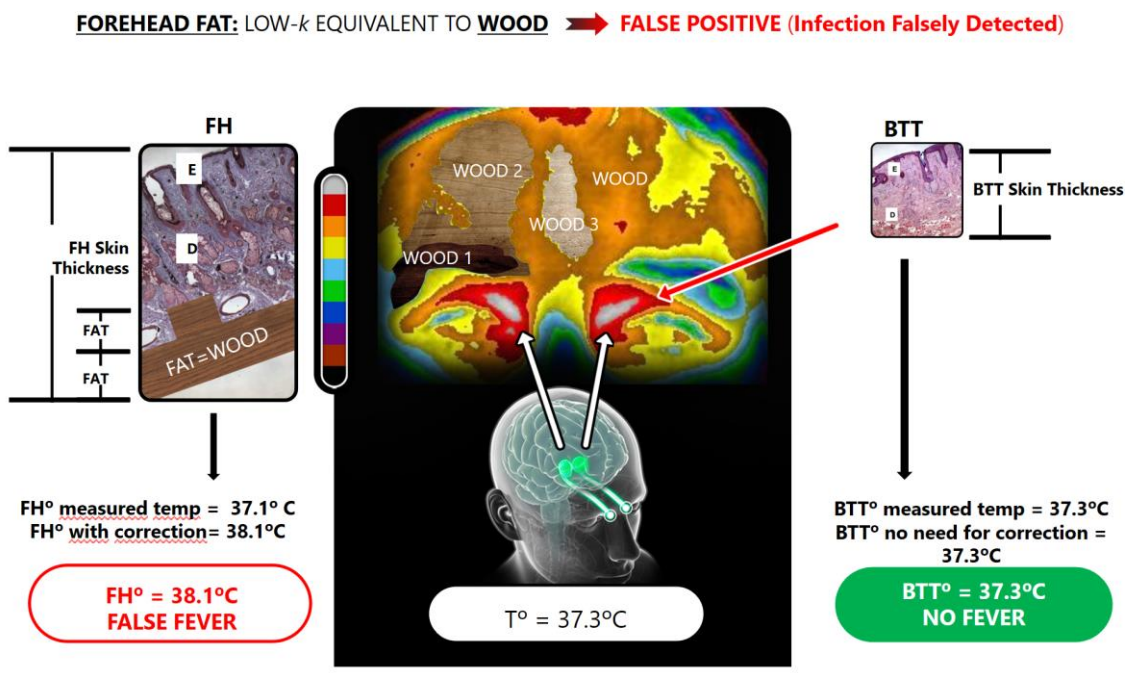

(**C**) Left panel shows thin wood representing thin fat layer in histological specimen, resulting in falsely high readings (due to correction factor). Comparative thickness between BTT and FH skin can be seen. Relatively thin fat layer results in overestimation (see text for details).

Section 5. Vasomotor tone response of high-*k* (BTT) and low-*k* surfaces and their epidemiologic implications for spreading COVID-19

To further confirm that widespread use of low-*k* thermometry is likely hastening the uncontrolled spread of COVID-19 worldwide by violating laws of physics and biology, through measurements on body surface with thermal conductivity as oak (**Wenger, 2002)** and that are characterized by the presence of an artery (which leads to countercurrent heat exchange with veins besides having highly reactive vascular tone), we assessed thermal emission response (of BTT and face) to externally induced activation of vasomotor tone. This experiment is also aimed to confirm that without an underlying tunnel, thermal emission via forehead, SPV or body skin and mucosal site beyond $SMOS_{BTT}$ cannot accurately correspond to the body thermal status, afebrile and febrile.

We tested impacts of dynamic challenges on thermal emission during facial fanning with a ventilator blowing air (speed of about 5 cm/sec, 13-15°C). Whereas underlying facial vasculature was incapable of maintaining thermal emission including the forehead, BTT emissions remained near baseline (**Figure 5A**) despite direct cooling of the skin and exposure to cooled blood in facial veins that enter SOV (**Abreu et al., 2020a**). Except for BTT site, temperature of all facial regions declined markedly over time **(a → d → h → l)** reaching about 4.0°C in the last frames after 24 min of exposure (2 min/frame). Even the forehead (and areas of SPV) declined to low levels, with forehead temperature (FH°) reduction of 2.0°C in 6 minutes [(**c**), green-dark blue] and over 3.5°C below baseline at end of study, shown in brown color. Such a dramatic change in temperature in

the context of a vasoconstrictive stimulus is consistent with the vasoresponsiveness of cutaneous vasodilation during a local pharmacologic challenge (**Silverman et al., 1987**). The increase in local skin temperature of 3.3°C in the thigh due to topical drug effect causing vasodilation matches the decrease in local skin temperature of 3.5°C in forehead due to thermal challenge causing vasoconstriction. This irrefutable response of cutaneous perfusion designed by nature cannot be predicted by algorithms or correction factors due to great variability in cutaneous vascular response and the amount of fat across different individuals (from thick multilayered to a single flat thin, as seen respectively in **Figure 4B** and **4C** respectively, and in **Figure 1D)**.

Even when fanning-induced thermal challenge reduced halo temperature, the center of the tunnel at $SMOS_{BTT}$ maintained the highest isotherm that had been identified at baseline, consistent with an undisturbed radiant beam from the brain. Resilience of BTT thermal emission during facial fanning in contrast to lowered emission at remaining of face is consistent with isolated head cooling not leading to brain cooling, as measured invasively via an intra-brain catheter (**Mariak et al., 1999**) and by acoustically evoked brain stem potentials (**Jessen & Kuhnen, 1992**).

As shown above, similar magnitude of cutaneous vascular response, with increase of 3.3°C (due to vasodilation) and decrease of 3.5°C (due to vasoconstriction) that occurred in completely distinct anatomic regions (thigh and forehead respectively), shows an agreement for large variation of cutaneous thermal response along the body surface, which reveals a staggering range of about 7.0°C in thermal variability in the surface of the human body, voiding thereby the ability of forehead, wrist, or any low-*k* skin site to provide reliable temperature measurements.

This large thermal swing further demonstrates variable and unpredictable thermal behavior of forehead, and further supports the inability of FH° (or low-*k* surface thermometry) to provide valid measurements needed to control COVID-19. According to sudden 2.0°C reduction of FH° shown above, a subject infected with COVID-19 having true temperature of 38.2°C, may change (due to variable skin vascular perfusion) to a reading of 36.2°C in mere 6 to 8 min, leading to false negative readings, causing the virus to go undetected, and if that occurs in large crowd settings and ports of entry (exemplarily shown below) may result in rapid and uncontrolled COVID-19 spreading, more commonly occurring in a second wave (**Ferguson et al., 2020; Moore et al., 2020**) known to be the deadliest (**Johnson & Mueller, 2002; Moore et al., 2020; Tomes, 2010**). This rapid thermal change coupled with the astonishing 7.0°C temperature variation on the surface of the human body (except eyelid at $SMOS_{BTT}$) coupled to baseline thermal status that reaches even 3.0°C lower than true brain thermal status (**Figure 3C,** showing cold "blue" forehead and hot "red-gray" $SMOS_{BTT}$), indicates that low-*k* surface thermometry (at forehead or any low-*k* body surface) would benefit from adjustment with the brain-based thermophysical conversion shown here) in the context of the necessary detection of thermal status to prevent COVID-19 spreading.

Considering that COVID-19 may rival the 1918 pandemic (**Gates, 2020**) that resulted in the catastrophic loss of 100 million lives and collapsed economies (**Johnson & Mueller, 2002; Tomes, 2010)**, it is vital to determine epidemiologic aspects for the rapid widespread of the virus, as occurred in 1918, such as large crowd settings relying on FH° or low-*k* surface thermometry, shown here by way of a sampling from around the world.

It was noted that the emergence of the outbreak in 1918 occurred in military camps in Europe and the final trigger for the pandemic was the interaction of troops with the general population (**Oxford et al., 2002; Oxford et al., 2005**). Although COVID-19 has different epidemiology than 1918, the same risk is present today for the uncontrolled COVID-19 spreading from settings, such as military bases, that tend to congregate thousands of people in close proximity or that live in close quarters. Dependence on forehead (low-*k*) thermometry in efforts to prevent

COVID-19 spreading and preserve lives is common place worldwide in high risk environments such as military bases (**Figures 5B-E**) as well as large crowd settings such as indoor concert (**Figure 5F**), work site (**Figure 5G**), factory (**Figure 5H**), amusement park (**Figure 5I**), outdoor setting (**Figures 5J,K**), hospital (**Figures 5L**), school (**Figures 5M,N**), and port of entry (**Figures 5O-T**), besides business (**Figure 5U**) and government facilities (**Figures 5V-X**). This underscores the vital importance of appreciating thermophysical insulatory barriers that may preclude clinically useful forehead (or low-*k* surface) measurement, that give a false sense of protection and security, unknowingly resulting in virus entry and spreading in such large crowd settings and from there to communities at large (despite the diligent temperature checking, as occurring around the world).

Likewise, other thermometry (e.g., tympanic, **Figure 5Y**), not in concert with biology and physics may lead to COVID-19 spreading despite temperature checking. Presence of something as trivial as ear wax, causes insulation in ear canal that impede access to the heat source, and many studies confirmed unreliability of ear thermometry (**Geijer et al., 2016; Mogensen et al., 2018; Niven et al., 2015; O'Brien et al., 2000**). Cerumen needs to be removed for proper measurement, which is not practical, besides having high risk of cross-contamination, with highly infective virus. Nonthermally configured sites as ear canal also conflict with biology since removal of wax impacts natural body protection as cerumen has antifungal and antibacterial function (**Lum et al., 2009**).

Figure 5. High-*k* (BTT) and low-*k* surfaces vascular response and epidemiological impact. Bar shows light emission grades (0.5°C/color), highest (gray) to lowest (brown-black).

Figure 5A

Vascular response of high-k BTT and low-k surfaces and their epidemiological impact

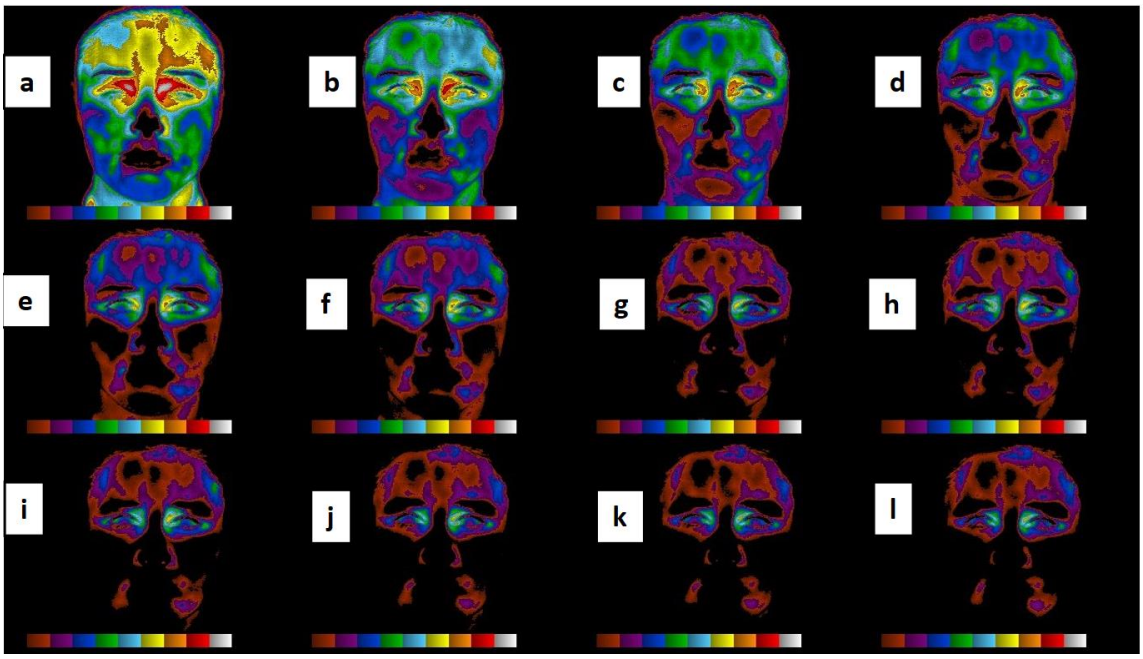

(**A**) Serial thermograms during fanning shows progressive facial cooling, from baseline (a) to coolest (l). BTT° remained close to baseline, other sites declined dramatically, even to very low absolute levels (<30°C, black zone). FH° and SPV declined to low temperature levels despite large STA (Figure 1C) and same fat-free histology as BTT (Figure 2A), respectively.

Figure 5B – Close Quarters, Large Crowd Setting
Low-k Forehead Temperature Check: North Carolina, **UNITED STATES | *MARINE BASE***

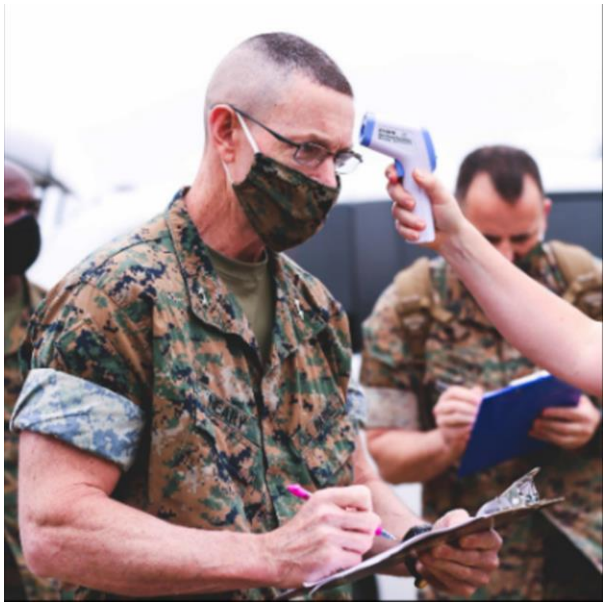

Major General Stephen M. Neary having temperature taken at Marine Corps Air Station, New River, NC on May 29, 2020. (**U.S. Department of Defense, Finnerty, 2020**).

1

Figure 5C – Close Quarters, Large Crowd Setting
Low-k Forehead Temperature Check: **RUSSIA | *MILITARY BASE***

A Russian conscript having temperature measured in Kalinigrad on May 20, 2020 (**Reuters, 2020**).

2

Figure 5D – Close Quarters, Large Crowd Setting
Low-k Forehead Temperature Check: **ISRAEL | *MILITARY BASE***

An Israeli soldier checks the temperature of a comrade as he enters a military base in March 2020 (**Davis, 2020**).

1

Figure 5E – Close Quarters, Large Crowd Setting
Low-k Forehead Temperature Check: Texas, **UNITED STATES | *ARMY BASE***

A soldier has his temperature taken at Fort Hood, Texas, July 13, 2020 (**Myers, 2020**).

2

Figure 5F – Close Quarters, Large Crowd Setting
Low-k Forehead Temperature Check: **GERMANY | *INDOOR CONCERT***

A participant has his temperature checked upon arrival at an indoor concert in Leipzig, Germany on August 22, 2020 (**Associated Press, 2020)**.

1

Figure 5G – Large Crowd Setting
Low-k Forehead Temperature Check: **CHINA | *WORK SITE***

A worker has his temperature checked at a construction site in Chongqing, China on February 29, 2020 (**Kun &Wenting, 2020**)

2

Figure 5H – Large Crowd Setting
Low-k Forehead Temperature Check: **FRANCE | *FACTORY***

A worker has his temperature checked at a Toyota Plant in Onnaing, France on April 21, 2020 **(Hindustan Times, 2020)**.

1

Figure 5I – Large Crowd Setting
Low-k Forehead Temperature Check: Florida, **UNITED STATES | *AMUSEMENT PARK***

A child has her temperature taken at an amusement park in Orlando, FL on July 15, 2020 **(Positively Osceola, 2020)**.

2

Figure 5J – Large Crowd Setting
Low-k Forehead Temperature Check: **AUSTRALIA | *OUTDOOR SETTING***

A child has their temperature checked in Australia on March 4, 2020 (**Jalal, 2020**).

1

Figure 5K – Large Crowd Setting
Low-k Forehead Temperature Check: **JAPAN | *OUTDOOR SETTING***

A participant has her temperature checked before a memorial service at the Peace Memorial Park in Itoman, Okinawa, Japan on June 23, 2020 **(Mori, 2020)**.

2

Figure 5L – Hospital
Low-k Forehead Temperature Check: Arizona, **UNITED STATES | *HOSPITAL***

An employee of Oro Valley Hospital has her temperature checked in Tucson, AZ on July 10, 2020 (**VOA News, 2020**).

1

Figure 5M - School
Low-k Forehead Temperature Check: Texas, **UNITED STATES | *HIGH SCHOOL***

Summer camp students have their temperatures checked by teachers at Wylie High School in Wylie, TX on July 14, 2020 (**CBS Austin, 2020**).

Figure 5N - School
Low-k Forehead Temperature Check: **RUSSIA | *CLASSROOM***

Students have their temperatures measured by a teacher in Moscow, Russia on September 7, 2020 (**Golovkin, 2020**).

1

Figure 5O – Port of Entry
Low-k Forehead Temperature Check: **MEXICO | *AIRPORT***

A passenger has her temperature checked at Benito Juarez International Airport in Mexico City, Mexico on March 13, 2020 (**McDonnel et al., 2020**).

2

Figure 5P – Port of Entry
Low-k Forehead Temperature Check: **ITALY | *TRAIN STATION***

A passenger has his temperature measured at a train station in Naples, Italy on April 4, 2020 (**Bendix, 2020**).

1

Figure 5Q – Port of Entry
Low-k Forehead Temperature Check: **NIGERIA | *AIRPORT***

A passenger has his temperature checked upon arrival at Murtala Muhammed International Airport in Lagos, Nigeria on February 27, 2020 (**Nordling, 2020**).

2

Figure 5R – Port of Entry
Low-k Forehead Temperature Check: **PAKISTAN | *TRAIN STATION***

A passenger has his temperature checked at a train station in Pakistan on March 18, 2020 (**Shams, 2020**).

1

Figure 5S – Port of Entry
Low-k Forehead Temperature Check: **HONG KONG | *TRAVEL CHECKPOINT***

A passenger has his temperature checked upon arrival to Hong Kong, China, on February 16, 2020 (**Today Online, 2020**).

2

Figure 5T – Port of Entry
Low-k Forehead Temperature Check: Alaska, **UNITED STATES | *AIRPORT***

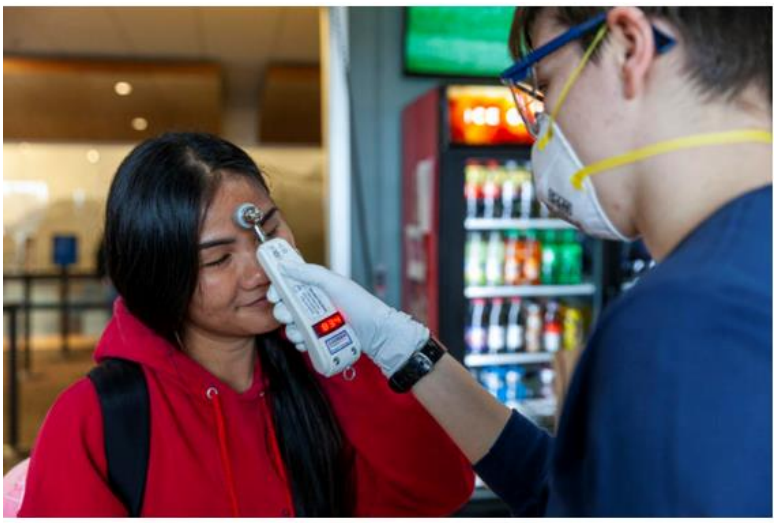

A passenger has her temperature checked at the Juneau International Airport in Juneau, AK on March 21, 2020 (**Baxter, 2020**).

1

Figure 5U - Business
Low-k Forehead Temperature Check: **BRAZIL | *RETAIL STORE***

A shopper has her temperature taken at a retail store in Sao Paulo, Brazil on June 10, 2020 (**Associated Press, 2020)**.

2

Figure 5V – Government Facility
Low-k Forehead Temperature Check: Washington, D.C., **UNITED STATES | *WHITE HOUSE***

A media member has his temperature checked by a member of the White House physician's office on March 15, 2020 (**Superville, 2020**).

1

Figure 5W – Government Facility
Low-k Forehead Temperature Check: **THAILAND | *GOVERNMENT BUILDING***

Thailand's Prime Minister Prayut Chan-o-cha has his temperature checked before a meeting in Bangkok, Thailand on March 2, 2020 (**Moritsugu, 2020**).

2

Figure 5X – Government Facility
Low-k Forehead Temperature Check: **RUSSIA | *ELECTION POLLING STATION***

A police officer has her temperature screened at a polling station during the 2020 Russian constitutional referendum in Vladivostok, Russia on June 25, 2020 (**Alamy, 2020**).

1

Figure 5Y
Tympanic (ear canal) Temperature Check: **GERMANY | *AIRPORT***

A Romanian seasonal worker has her temperature screened after landing at Hahn Airport in Hahn, Germany on April 13, 2020 (**Agence France-Presse, 2020**).

Section 6. Dominant vs Nondominant Cerebral Hemispheres Studies

In light of the greater temperature response of the left BTT° to bilateral seizures (**Abreu et al., 2020b**), we sought to determine if BTT° is selective for the brain near its internal terminus [shown to include ipsilateral brain lobes and peri-hypothalamic triunal (**Abreu et al., 2020a**)] by quantifying resting BTT° differences ipsilateral to the dominant and nondominant cerebral hemispheres (self-reported, investigator blinded to handedness) in 55 resting volunteers. In right-handed subjects (left brain dominant, n=44), Left BTT° was 36.19±0.4°C and Right BTT° was 36.05±0.4°C ($P<0.001$ for the 0.14°C difference). In left-handed subjects (n=9), Right BTT° was 36.43±0.2°C and Left BTT° was 36.26±0.3°C ($P<0.001$ for the 0.17°C difference). BTT° of dominant side was greater in 48 of the 55 subjects and equal to nondominant in 5 of the subjects. Two volunteers were excluded from analysis because they reported being ambidextrous. These findings strongly indicate that temperature of the brain near the BTT terminus generates the thermal signal via the right or left BTT. Our ongoing investigations showed difference of even 0.5°C, indicating that temperature measurements should be performed according to cerebral dominance to detect thermal changes associated with rise in temperature due to an infection (shown in companion manuscript). Thus, right-handed populations showed have temperature taken at the BTT of the left side, and left-handed populations showed have temperature taken at the BTT of the right side, which is used in the signal conversion (presented in the discussion).

Section 7. Consistency of BTT thermal emission across different races

Skin histomorphometry at $SMOS_{BTT}$ revealed equivalent dimensions and structure for various races (**Abreu et al., 2020a**). Thermal emission, shown in representative Asian, Black and White subjects (**Figure 7A**), confirmed the morphologic features. BTT emission is consistently present in the eyelid at $SMOS_{BTT}$ (red area) while the forehead and remaining facial areas are silent in relation to high thermal emission areas. Thus, BTT° uniquely enables achieving consistent temperature measurements across different races, which is essential in the global context of the COVID-19 pandemic.

Figure 7A

Consistency of BTT thermal emission across different races

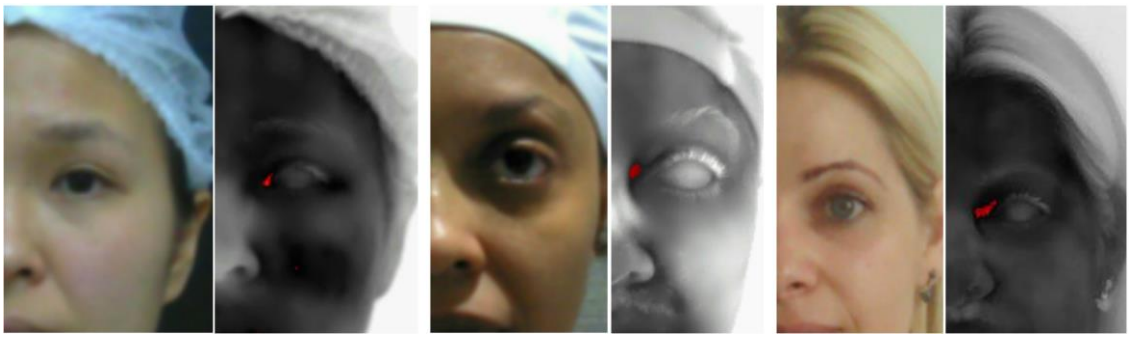

(**A**) Comparative IR light emission in different races showing highest intensity at the BTT site (red zone at medial eyelid) and no equivalent thermal energy on FH and face in all subjects.

Section 8. Practical Recommendations for Thermometry and Screening in the context of COVID-19 based on the BTT signal and thermodynamics

Integration of thermoanatomy, histomorphometry, thermal emission and thermometry have delineated features of the BTT and surface sites throughout the forehead and face. The findings can be converted to guidelines which can be promptly implemented for individual temperature assessment and mass screening. (1) Hemisphere Dominance is a key point: our cerebral hemisphere dominance studies revealed distinct brain thermodynamics with higher temperature according to cerebral dominance. Thus, cerebral dominance should be taken into consideration during screening, with separation of left- and right-handed individuals and positioning the thermal imaging detector or thermometer accordingly (e.g., left BTT for right handed populations). (2) A second point is removal of eyeglasses, which is needed in order to optimize mass screening at airports and ports of entry, which maybe vitally needed in the reopening the economy and travelling. As observed in **Figure 8A**, the use of eyeglasses or sunglasses block the BTT site (reducing temperature by 1.18°C with sunglasses and 1.15°C with prescription eyeglasses). Hence, authorities should ask for removal of eyewear prior to screening or thermal imaging detection. (3) Site: thermal emissive screening should encompass the BTT site, which is not affected by blinking or eye closure, or eye secretions, as occur with the ocular mucosa and inner canthi. The BTT signal requires a view of the detector that encompasses the medial upper eyelid preferably from a lateral 45-degree angle position (at about 1 inch from eyelid surface for non-contact infrared thermometry), a move from a low-*k* forehead to a high-*k* radiant eyelid.

Figure 8A

Impact of eyeglasses on thermal emission

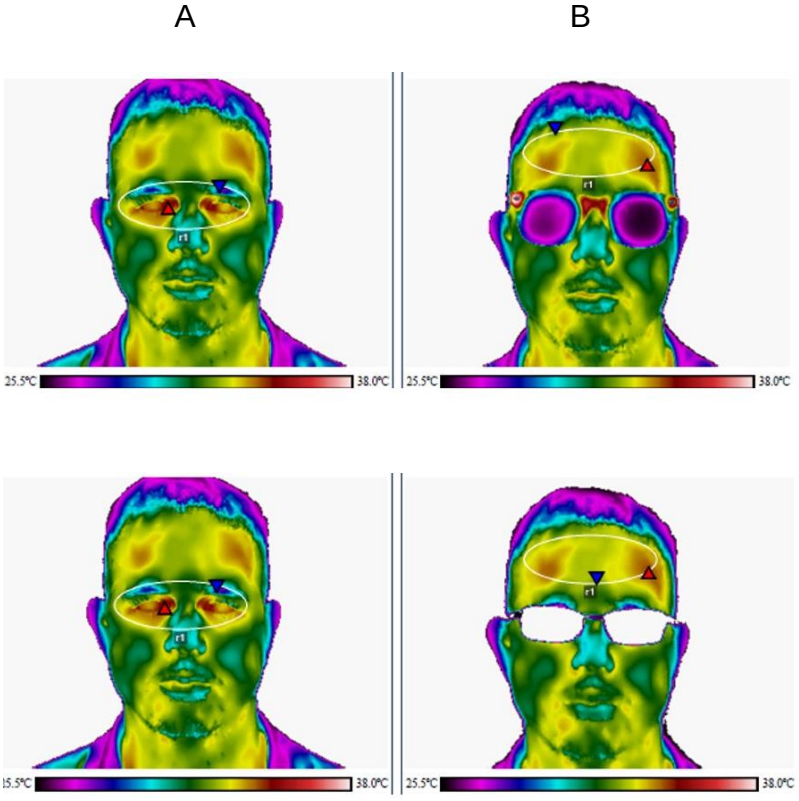

(A) Impact of eyewear on thermal emissive screening, eyeglasses move the highest thermal emission zone (oval) from BTT to forehead by frame and lens blocking the BTT site. Image A: thermal emission showing temperature at the BTT site of 35.43°C without any type of eyeglasses. Image B (thermal emission with eyeglasses blocking BTT emission): temperature of 34.30°C from the hottest facial site for prescription eyeglasses and 34.35°C for sunglasses (see text for details).

Discussion

Until now, the battle against COVID-19 has been constrained by temperature measurements not aligned with physics and biology and by heretofore unattainable noninvasive measurement of brain (and body core) temperature (**Moran & Mendal, 2002; Robinson, 2004**).

Thermometric deficiencies and measurements not in concert with thermal physics and biology. Despite the invention of thermometers over 300 years ago, for centuries humans have invaded multiple orifices and used multiple sites in failed attempts to try to conquer the body's thermal barriers. And methods for measuring body core temperature today, that are being used during the COVID-19 pandemic, are still based on principles used in the middle of the 18th century (**Moran & Mendal, 2002**). Although electronic thermometers were developed, biological and thermophysical challenges result in widespread deficiencies and suboptimal results from forehead measurements and by other thermometry, which have been documented over time (**Farnell et al., 2005; Forrest et al., 2017; Geijer et al., 2016; Jensen et al., 2000; Kiekkas et al., 2016; Kiekkas et al., 2019; Kimberger et al., 2007 ; Latman et al., 2001; Modell et al., 1998; Mogensen et al., 2018; Niven et al., 2015; O'Brien et al., 2000; O'Grady et al., 2008; Patel et al., 1996 ; Suleman et al., 2002; Tandberg & Sklar, 1983; Teller et al., 2013; Varney et al., 2002)**. This thereby significantly impacts the ability of current thermometry to effectively control COVID-19.

Temperature monitoring traditionally has relied on sites not biologically configured for temperature measurement, thereby producing widely variable and unreliable results, and thus precluding containment of the COVID-19 pandemic. Accessed skin sites (such as forehead, axilla, wrist, and other surface areas) are structured for thermal insulation, not the transmission of heat (**Sections 1 and 2**). Except for skin of $SMOS_{BTT}$, the entire body is covered by a thermal insulatory wall, including layers of largely variable structure and size, such as fat [k = 0.00004 Kcal/(s·N·C)] and dermis [k = 0.00004 Kcal/(s·N·C)], noted before, that prevents reliable skin-based measurement of brain (or body core) temperature. Corrective algorithms lack reliability due to variations in insulatory layers among individuals, spatial variability among sites on the same individual, and temporal variability at the same location, beside vascular perfusion changes leading to even 7.0°C variability of skin temperature (**Section 5**), failing thereby to achieve the necessary clinical accuracy and reproducibility of measurements needed to control the COVID-19 pandemic. Internal sites such as the mouth, esophagus, nasopharynx, ear, rectum, and bladder are structured for ingestion, air exchange, auditory sensation, and excretion, Their contents—food, feces, liquid, air—may also hamper accurate thermometry readings. In addition, invading the body comes at a great cost, including risk for injury (even potentially fatal complication as esophageal and rectal perforation) and incorrect sensor position because the location of the probe cannot be viewed during measurement. Despite Core° acquiring more reliable measurement as compared to surface sites, it does not represent brain temperature (**Abreu et al., 2020b**). Moreover, invading the body by any means increases the risk of spreading COVID-19 and prevents the safe use of invasive thermometry in the context of a pandemic.

As demonstrated herein with morphologic, thermophysical, and clinical assessments, forehead thermometry is suboptimal from both physical and biologic standpoints, besides failing to detect early thermoregulatory changes, which is necessary to successfully detect COVID-19.

Whereas BTT° monitoring captures undisturbed brain thermal signals without the need for a correction factor, the anatomy, histology and thermophysical barriers of the forehead warrants correction factors. This latter approach tends to overestimate temperature in attempts to offset the body's low-*k* barrier. Moreover, by being exposed to ambient temperature (in sharp contrast to the BTT° that is shielded inside the skull), results may simply represent external temperature and/or influences of the environment, resulting in false positive readings in a hot environment, such as a hot day in the summer (due to a combined effect of vasodilation and warm skin temperature) and false negative readings in cool or cold environments, such as with exposure to air conditioning (in a car or facility) prior to a temperature check (due to a combined effect of vasoconstriction and cold skin temperature). In addition, variable fat layers, the dermis, vasculature, and vasomotor tone in the forehead further exacerbates overestimation and underestimation of temperature and provides unreliable and inconsistent measurements. This is especially true near the fever threshold, even when scanning and a correction factor is employed, as extensively documented by multiple authorities over two decades (**Forrest et al., 2017; Geijer et al., 2016; Kiekkas et al., 2016; Kiekkas et al., 2019; Kimberger et al., 2007; Mogensen et al., 2018; Niven et al., 2015; Patel et al., 1996; Suleman et al., 2002; Teller et al., 2013**).

Temperature measurements violating physics and biology arguably may well lead to undue expansion and duration of the COVID-19 pandemic. Healthy individuals misdiagnosed as febrile due to overestimation are unnecessarily quarantined and/or placed with infected individuals (in households, hospitals, or quarantine facilities) leading to more contagion as healthy populations become infected. In addition to injuring healthy individuals and further spreading COVID-19, unnecessary incidents of quarantine or hospital visits are an undisputable and costly strain to health care systems, resulting also in a reduced workforce with obvious socio-economic consequences. Conversely, underestimation with surface thermometers occurs due to low-*k* at the skin surface and the related vascular physiology. Our morphologic, emissive, and clinical data indicate that diverse fat layers in the forehead across different individuals (**Figure 1D**) may lead to deficient fever detection. False negative readings may lead to uncontrolled virus spread [again, even in settings monitoring temperature (**Figures 5B-Y**), potentially leading to rapid spread in crowded facilities such as schools, entertaining venues, and military bases. Additionally, underestimation of body core temperature delays seeking care, leading to increased mortality, morbidity and sequela. Forehead thermometry is impacted even by emotions due to unpredictable and variable vasomotor tone, leading to compounding effect of overestimation or underestimation. Mass screening by thermal imaging also suffers from comparable deficiencies for infection detection (**Priest et al., 2011**).

Measurement in nonthermally configured sites (e.g., ear thermometry, tympanic membrane) also may conflict with natural body protection. As shown, cerumen has antifungal and antibacterial function (**Lum et al., 2009**); but the protective wax impedes access to the heat source and must be removed for proper measurement of temperature in the ear. In addition, oral thermometry requires at least a 30-minute wait after food or liquid is consumed, otherwise the measurements will provide an erroneous reading (**Quatrara et al., 2007**). This is particularly problematic when consistent fluid intake is recommended by the CDC since hydration is key for those infected with COVID-19. Moreover, measurements in sites not biologically configured are in conflict even with main physiological parameters during fever: such as tachypnea (rapid breathing), which occurs during fever and falsely reduces oral temperature (**Tandberg & Sklar, 1983**); whereas bradypnea causes false temperature elevation (**Quatrara et al. 2007**), thereby changes in respiratory function may lead to false negative and positive readings, respectively.

The limitations of current thermometry are "built" upon a foundation of thermometric deficiencies that has led to "a confusing jungle of sites and technologies" (**Robinson, 2004**), and humanity cannot attack an opponent as infective and deadly as SARS-CoV-2 by relying on jungle of confusion. More than 50 years after the publication of the classic article on etiologies of "fever of unknown origin" (**Petersdorf & Beeson, 1961**), inadequate thermometry remains a recognized constant reality, and we are still faced with the dilemma of "fever of unknown degree". Doctors (and patients) often have been saddled with the basic, but nonetheless vital, question: "Does the patient have fever?" as one site indicates normothermia and another simultaneously indicates fever. Thus, the deficiencies in temperature measurement have prevented medicine from answering even the most basic question, with practitioners pleading "Can there be a standard for temperature measurement…?" (**Martin & Kline, 2004**). Children are particularly likely to be misdiagnosed due to suboptimal thermometry during the COVID-19 pandemic because of parental dependence on the only main objective warning sign for COVID-19 (or Kawasaki disease), which is fever. The other signs are subjective and difficult to interpret, such as fast breathing, not drinking enough fluids, bluish color, or irritability. Wrong thermometry jeopardizes children in two ways – lack of detection, which can lead to complications and possibly death, whereas false fever, may expose children to disease while seeking medical attention. In addition, an invalid reading can fail to identify an asymptomatic child who has the potential to shed virus.

Until discovery and characterization of the BTT with its direct thermal connection with the brain thermoregulatory center (**Abreu et al., 2020a**), the thermal signal from our most vital organ appeared to remain trapped within the cranium. The current limitations have forced practitioners and the public to navigate in a confusing thermometric jungle (**Robinson, 2004**) while a standard for body temperature measurement remains to be found.

A key question. Hence, what differentiates BTT° from joining the stockpile of failed devices and body sites that has characterized the history of thermometry for over 300 years and that have been used in pandemics for centuries, and currently utilized with COVID-19? We believe the answer is simple: whereas, for centuries, thermometry at other sites, used in all settings, from households to hospitals, must overcome physics, physiology and biology, BTT thermometry is the only method in concert with the laws that govern nature (thermodynamics) and life (biology). The thermodynamics governing the BTT and temperature measurement via a thermophysical tunnel across high-*k* radiant eyelid enabled our harnessing engineering provided by nature, as opposed to imposing human engineering on nature, as has occurred since the beginning of thermometry.

High-k brain thermometry and measurements according to thermal physics and biology (BTT). The brain is a thermodynamic organ (**Collell & Fauquet, 2015**) and the BTT has no function other than thermal, working as a natural brain temperature indicator through a thermophysical path in harmony with morphology (connection with brain), physiology (stable blood volume and signal unaffected by respiratory changes) and physics (low-*k* wall encircling high heat capacity medium with high-*k* terminus) (**Abreu et al., 2020a; Abreu at al., 2020b**). This naturally engineered waveguide enables detecting and quantifying brain/core discordance, and heretofore unattainable distinction between brain and body core values.

The clinical experiments and observations reported have provided evidence that, as a component of the peri-hypothalamic thermoregulatory triune, signals traversing the BTT are in continuum with thermal changes associated with hypothalamic activity. Hence, the apparent aberrancies of vein, fat, bone, and skin have provided a tunnel which enables unopposed capture of brain thermal signals, which in the context of COVID-19 results in a BTT-based signal conversion that may reveal thermal response to onset of infection.

Public health officials, professionals, businesses, communities and populations around the world are making decisions as to the presence of fever for protection against COVID-19 based on measuring temperature on or over the lowest thermal conductivity tissue (fat) and in an highly reactive vascular region that leads to instantly great variations of temperature. Thermo-emissive imaging or non-contact thermometry that is aimed at the $SMOS_{BTT}$ should markedly improve the accuracy and consistency during screening for fever at airports, ports of entry, and large crowd settings (cited exemplarily above) by providing a site that is void of confounding levels of fat and dermis and inconsistent degrees of vascular distribution and vasoreactivity. In addition, in view of brain thermal signal, in the presence of a pyrogen (e.g., viral pathogen) is upward, measuring temperature at the $SMOS_{BTT}$ is more likely than conventional screening to identify patients with subclinical (e.g., pre-febrile) as well as clinical (febrile) illness.

Thermometry that embraces measurements on low-k surfaces and high reactive vascular regions, leading to false-negative and false-positive readings, reinforces the virus's ability to spread and ravage humankind. This stresses the urgency for rapid intervention. As an initial application of findings herein, we recommend moving the measurement site (which can be implemented by any nation or community in the world) from above to below our gracile brow ridge, a move from a low-k dark forehead (overlying a fat-laden barrier) to a high-k radiant eyelid (above a brain↔surface tunnel).

It is important to note that measurement at the BTT site with a forehead thermometer or any thermometer with a correction factor will most likely lead to falsely high readings due to a high-*k* surface overlying a high thermal capacity tunnel, in addition to lack of proper angle and field of view that are necessary for non-contact measurements at the BTT site (as shown below). And to be useful, when possible, correction factors need to be eliminated.

BTT-enabled signal conversion. Despite billions of temperature measurements being performed daily worldwide (exemplarily shown in **Figures 5B-Y**), COVID-19 relentlessly continues to spread, devastating the physical, emotional, and financial health of the world, reaching the catastrophic milestone of over one million lives lost. Here we propose a BTT-enabled signal conversion to optimize low-*k* thermometry to detect febrile state and more effectively control COVID-19, without any cost whatsoever or undue burden, based on our long term understanding of viral infections in tandem with brain temperature.

During the SARS outbreak, right after Yale University presentation of the BTT as first methodology to noninvasively measure brain temperature (**Yale University, 2003**), and preliminary BTT description (as thermophysical path providing a metric consistent with Stefan-Boltzmann's law of black body radiance) (**Abreu, 2002**), Chinese colleagues collaborating with us reported that BTT monitoring systems *"…could also be used to detect diseases such as the flu-like SARS (severe acute respiratory syndrome) that spread early this year to about 30 countries…*" (**China Daily, 2003; China.org.cn - Xinhua Agency, 2003**). Eradication of SARS precluded continued collaborative efforts with Chinese colleagues, nonetheless, to effectively establish the foundation for detecting any coronavirus infection with BTT-based methods, we first performed extensive anesthesia, surgical, neurological, fever, hypothalamic response, and brain thermodynamics studies. We recently reported that BTT° follows brain during brain/core discordance due to neuronal activity (**Abreu et al., 2020b**), which provides key information for the brain-based signal conversion introduced here in accordance with thermal physics and biology.

Our continued work on detecting infection based on BTT-enabled signals using artificial intelligence started in 2017, which provided key knowledge for the herein simplified proposed signal conversion. With the goals of preventing COVID-19 spreading and preserving lives during

infections, as part of our current all-out effort against COVID-19, we redirected intelligence acquired previously [which are described in detail elsewhere (**Microsoft, 2017**)] to provide a simple and straightforward conversion signal to enhance current low-*k* thermometry, which can be immediately used freely by any country, community or individual in the world.

Considering the worldwide daily reliance on forehead thermometry (**Figures 5B-X**), and our objective to provide actionable information to help control the COVID-19 pandemic, which can be implemented anywhere, from homes to hospitals, we provide here guidelines, with the goal to optimize measurements done on low-*k* skin (of the forehead). In the context of appreciation of hypothalamic connection and of barrier-free measurement via skin overlying the BTT, **Table 3** provides a foundation for applying the present findings to improve the utility of currently disappointing assessment of FH° as a screening tool.

The signal conversion proposed here is accomplished by a dual sequential measurements, first at forehead then at the BTT site, according to the following steps: (1) Determine cerebral dominance and direct the thermometer to the dominant cerebral hemisphere; (2) Perform forehead measurement with thermometer having correction factor (CF) according to dominant hemisphere (left side for right-handed individuals and vice-versa); (3) Perform measurement at the BTT site using the same forehead thermometer (left BTT for right-handed individuals and vice-versa), just moving from forehead to the upper eyelid adjacent to the nose, and positioning the detector in a diagonal 45 degree angle view that is pointing at the intersection of nose and eyebrow, just below the eyebrow at the upper medial eyelid skin [that is the BTT site, described previously (**Abreu et al., 2020a**)], and (4) Follow the instructions according to the signal conversion table below.

Table 3. Signal Conversion. Dual Sequential Measurement for Optimizing Detection of Fever Obtained by Traditional Forehead Thermometry with Second Measurement at the BTT site using Same Forehead Thermometer

FH◦	**Concerns**	**Second Measurement at BTT Site**
≥ 38°C	Suggestive of fever, but may represent false positive for fever if CF is excessive for given setting (e.g., subject, site, vasomotor status)	--If BTT° <38°C, suspect that FH° is a false positive for fever; further assessments should be pursued --If measurement at BTT° >38° C, then consistent with fever (most accurate if one knows the magnitude of the CF)
< 38°C	Suggests absence of fever, but may represent false negative if CF is insufficient for given setting (thick fat layers)	--If BTT° is between 38.4°C to 38.6°C, one should suspect fever; --If BTT° above 38.7°C, this indicates fever is likely --If BTT° < 38°C, the subject is afebrile

Although this signal conversion based on a high-*k* surface aligned with hypothalamic thermal source may optimize the values obtained on low-*k* surfaces (not connected with brain), we emphasize that this signal conversion and guidance has limitations since it is not possible to determine the amount of fat or dermis thickness of the forehead (intersubject and intrasubject), and thus the forehead remains an indeterminate thermal barrier. Moreover, forehead vascular reactivity

may impact measurements, as well as large number of unknown correction factors and algorithms used in different thermometers. Nonetheless, conversion of a low-*k* to a high-*k* surface, as shown here, provides a more clinically meaningful temperature measurement at the forehead.

Early infection detection, as provided by signal conversion described herein, enables early therapy, which may prove to be vital for achieving effective treatment. If an infected person falls into the group associated with high risk for complications or starts to experience symptoms, therapeutic approaches may be immediately implemented with standard available pharmacological and chemically-based therapies, which are shown to have good therapeutic response if started in the early stages of infection (**Arshad et al., 2020; Beigel et al., 2020; Chan et al., 2003; Risch, 2020; Soo et al., 2004; Vastag, 2003**).

In concert with those readily actionable means to identify fever, studies are being initiated to identify the prefebrile as well as febrile phases of viral illness by characterizing the thermodynamic patterns transmitted by the BTT to sensors designed to capture BTT° without confounding correction factors and algorithms that are required at all other surface sites to counter the impact of the body's thermal barrier and the inconsistencies caused by vasomotor activity.

There is light at the end of the brain tunnel, which reflects undisturbed tunneling transmission of brain thermal energy through overcoming for the first time the body's thermal barrier. We herein have shown how the unique thermoconfigurative properties of the skin of the medial eyelid at the $SMOS_{BTT}$ and the fat-encased course of the SOV between this site and the cavernous sinus emits the highest intensity light on body surface and provide the biophysical basis for controlling COVID-19. In light of world dependence on temperature assessment, we have adapted our findings to: introduce immediately actionable processes that will enable thermo-emission to more accurately and consistently detect fever, by encompassing the $SMOS_{BTT}$ within the imaging window; and enable virtually all thermometers and related sensors designed for use at other sites to likewise more accurately detect fever, with concomitant monitoring at the $SMOS_{BTT}$.

The discovery of the BTT and our numerous investigations here unearthed the hypothalamus, which until now seems to be trapped inside the cranium, and enabled addressing the fundamental precept put forth by Lord Kelvin: "You cannot manage what you cannot measure" (**Scripture, 1892**). To effectively manage the COVID-19 pandemic, we may add: to measure accurately and precisely using signals received from an error-free source (the human brain) from a natural waveguide and its high-*k* eyelid terminus. This may constitute a hinge moment in the combat of a pandemic by bringing for the first time the integrated morphology and thermal physics of a brain radiant eyelid thermal waveguide for preserving lives threatened by COVID-19 around the world.

By harnessing the unrivaled power of combining the force that governs nature (thermodynamics) with the most powerful system in nature (the human brain) our ongoing investigations show that the end of the pandemic is within reach. The findings herein enables humanity to escape dependence on surface measurements across thermal barriers and highly reactive vascular regions, to bring an end to the period in history in which the world measured human body temperature on or over a low-*k* surface, which is fraught with errors and limitations that humanity cannot afford if it were to effectively combat and defeat COVID-19, or any other deadly virus that may strike the human race (**Sun et al., 2020**).

Materials and Methods

Approvals and Consents. The studies were reviewed and approved by authorized ethics committees in accordance with the relevant guidelines of the Institutional Review Board of the

Yale University School of Medicine. Informed consent was obtained from participants after a full description of study procedures, risks, and potential benefits prior to participation.

Tissue Preparation and Analysis. Anatomo-histologic studies were performed in 13 adult cadavers, which were fixed in 4% formaldehyde solution. Intravascular injection of stained Neoprene® was made according to standard procedures to make evident the venous and arterial systems. Photomicrographs were obtained with a Carl Zeiss Axiovision microscope with digital imaging and Zeiss lenses 10X e 40X. Dissections were performed through the orbital bone walls to show the SOV, orbital fat and their anatomical relationships. Intracranial dissections were performed to expose the intracranial portion of the SOV and the neighboring vessels communicating via the cavernous sinus (components of the triunal system) using axial cuts and parasagittal cuts. Facial dissections included removal of the skin for exposing arterial and venous networks. Histologic studies and measurements (in a micrometer scale) were performed in skin fragments. Specimens supplied from the medial eyelid were embedded in paraffin, 7 mμ sectioned and stained with haematoxylin-eosin. All anatomic and histologic studies were performed in accordance to relevant guidelines of the Paulista School of Medicine of the Federal University of Sao Paulo.

Thermal imaging studies: infrared light was captured from the face, neck and BTT region, in a controlled temperature (20-22°C) draft-free room. Sections 1 to 6: TyTron C500IR, Titronics R&D, Tiffin, Iowa, USA. Specifications for the analyses were as follows: image temperature range of 8ºC (gradient indicated in view by bar on right with highest at top), infrared spectral range of 7.5-13 microns, absolute resolution of 76,800 IR sensors, spatial resolution of 1.3 mrad, and thermal sensitivity of 0.08°C. A computerized isotherm analysis of the gray scale images was performed. The hottest area on the image was demarcated with a red isotherm. The warmest nonadjacent site was demarcated with a green isotherm. Comparison between the temperatures of these sites was performed using two-tailed paired t-test. The heterogeneity of readings is displayed in Table 1. Distribution of red and green isotherms is quantified according to the dimension in each cell of the grid superimposed on the gray scale images. Sections 7 and 8: Device: FLIR Termocam Medical, FLIR, USA. Software: VisionFY, ThermoFy, University of Sao Paulo School of Medicine, Brazil.

Comparative temperature measurements in normal resting subjects: (1) BTT°, Core° (SL°) and Surface° comparative measurements: measurements were performed in 18 normal volunteers who were requested to refrain from eating or drinking for 30 min before being studied while sitting comfortably in a room after a five minutes stabilization period. Sites were compared on 5 separate days, using equally calibrated thermistors, and without any offset or correction factor. SL° measurements used a bare thermistor placed on the sublingual pocket. The consistency of BTT° and SL° under resting conditions was assessed with bias (and 95% limits of agreement corrected for repeated measures), and (2) Cerebral hemisphere dominance: in the cerebral dominance studies performed in 55 subjects (23 female, 22 male), the left BTT° and right BTT° were measured using a surface BTT sensor (Abreu BTT C1 sensor, BTT Corp, Aventura, FL) divided in one group with 44 right-handed subjects and a second group with 9 left-handed subjects (two other subjects reported being ambidextrous). Evaluators were blinded as to subject handedness. Values are expressed as mean±SD; differences were analysed with 2-tailed paired t-test.

Data availability: datasets generated during the studies are available upon request**.**

Supplemental information *(movies*) is included with this manuscript.

Acknowledgements. Special thanks to Dr. Roberta Hines of the Department of Anesthesiology at Yale School of Medicine for allocating personnel and resources. We thank the Department of Ophthalmology and Visual Science of the Yale School of Medicine, and its former chairman Dr. M.

Bruce Shields for support, guidance and reviewing the comprehensive manuscript; the Department of Morphology and Genetics of Paulista School of Medicine of the Federal University of Sao Paulo, Brazil for anatomic and histologic preparations; and BTTCorp.com for providing equipment and sensors. We also thank Dr. Michael F. Bergeron for initial suggestions for the manuscript, Dr. William C. Amalu for assistance with thermal images and videos, Dr. Marcos L. Brioschi for assistance with thermographic screening and racial comparison, Robert Drew Singleton for editing and formatting of citations and figures, and Lauren Johnson for editing, assembly and formatting reference materials.

Author contributions. M.M.A. discovered the BTT and delineated thermophysical configurations. M.M.A. and D.G.S. contributed to design of all research protocols and collected the data for the various studies, analyzed all results, wrote the manuscript, and integrated the different components of this multidisciplinary investigation. R.L.S. jointly with M.M.A dissected cadavers; in addition, R.L.S. performed histologic and correlational studies, and associated data analysis. T.M.B. contributed to design, performance and analysis of cerebral hemisphere dominance. A.L.C. collected and analyzed data for thermometry correlation studies. A.S.H. contributed to anatomic and thermographic analysis. T.J.S. contributed to design of grid, data collection, and analyzed results. F.D. designed statistical methodologies and analyzed data.

Competing interests. M.M.A. holds patents on temperature measuring devices. All other authors declare that they have no competing interests.

References

Abreu, M. M., Smith, R. L., Ruskin, K., Silva, A. F., Haddadin, A. S., Bergeron, M. F., . . . Silverman, D. G. (2020a). Previously unseen brain-eyelid thermal tunnel reveals biological waveguide and transorbital thermophysical pathway to the brain. *Authorea*. doi:10.22541/au.160225723.36016917/v1

Abreu, M. M., Banack, T. M., Haddadin, A. S., Silverman, T. J., Dai, F., Elefteriades, J. A., . . . Silverman, D. G. (2020b). Brain/core Discordance due to Neuronal Activity Identified by Noninvasive Brain Temperature Measurement via Brain-eyelid Thermal Tunnels. *Authorea*. doi:10.22541/au.160315282.27681781/v1

Abreu, M. M. (2002). U.S. Patent No. *7187960* issued in 2007. Patent application filed on April 22nd, 2002. Washington, DC: U.S. Patent and Trademark Office.

Alamy. (2020, June 25). Stock Photo. Retrieved October 23, 2020, from https://www.alamy.com/vladivostok-russia-june-25-2020-a-police-officer-in-a-face-mask-has-her-temperature-screened-at-a-polling-station-during-the-2020-russian-constitutional-referendum-in-the-city-of-vladivostok-in-russias-far-east-most-regions-of-russia-will-vote-in-the-referendum-on-proposed-amendments-to-the-russian-constitution-from-25-june-to-1-july-2020-some-of-the-proposed-changes-raise-social-obligations-aimed-at-improving-living-standards-to-the-level-of-constitutional-norms-credit-itar-tass-news-agencyalamy-live-news-image364069013.html

Arons, M. M., Hatfield, K. M., Reddy, S. C., Kimball, A., James, A., Jacobs, J. R., . . . Jernigan, J. A. (2020). Presymptomatic SARS-CoV-2 Infections and Transmission in a Skilled Nursing Facility. *New England Journal of* Medicine, *382*(22), 2081-2090. doi:10.1056/nejmoa2008457

Arshad, S., Kilgore, P., Chaudhry, Z. S., Jacobsen, G., Wang, D. D., Huitsing, K., . . . Reyes, K. (2020). Treatment with hydroxychloroquine, azithromycin, and combination in patients hospitalized with COVID-19. *International Journal of Infectious Diseases*, *97*, 396-403. doi:10.1016/j.ijid.2020.06.099

Associated Press. (2020, June 10). Brazil Begins Reopening After 2-Month Coronavirus Shutdown. Retrieved September 14, 2020, from https://www.voanews.com/covid-19-pandemic/brazil-begins-reopening-after-2-month-coronavirus-shutdown

Associated Press. (2020, August 22). World hits grim COVID-19 milestone with 800,000 confirmed deaths. Retrieved October 22, 2020, from https://www.cbc.ca/news/world/coronavirus-covid19-world-aug-22-1.5696347

Baxter, A. (2020, March 20). Voluntary screenings begin at Juneau airport as local leaders advise would-be travelers to stay home. Retrieved September 11, 2020, from https://www.ktoo.org/2020/03/20/voluntary-screenings-begin-at-juneau-airport-as-local-leaders-advise-would-be-travelers-to-stay-home/

Beigel, J. H., Tomashek, K. M., Dodd, L. E., Mehta, A. K., Zingman, B. S., Kalil, A. C., . . . Lane, H. C. (2020). Remdesivir for the Treatment of Covid-19 — Preliminary Report. *New England Journal of Medicine*

Bendix, A. (2020, June 17). US states are instituting temperature checks at offices and restaurants, but a quarter of coronavirus patients don't develop a fever. Retrieved September 13, 2020, from https://www.businessinsider.com/temperature-checks-flawed-coronavirus-cases-asymptomatic-no-fever-2020-5

Benzinger, T. H. (1969). Clinical Temperature. *JAMA*, *209*(8), 1200-1206. doi:10.1001/jama.1969.03160210032008

Bergen, M. P. (1981). A literature review of the vascular system in the human orbit. *Acta Morphol Neerl Scand*, 19(4), 273-305.

CBS Austin. (2020, July 24). Nearly 100 babies have tested positive for COVID-19 in Travis County. Retrieved September 12, 2020, from https://cbsaustin.com/news/local/nearly-100-babies-have-tested-positive-for-covid-19-in-travis-county

CDC. (2017, March 21). Definitions of Signs, Symptoms, and Conditions of Ill Travelers. Retrieved August 12, 2020, from https://www.cdc.gov/quarantine/maritime/definitions-signs-symptoms-conditions-ill-travelers.html

CDC. (2020, May 13). Symptoms of Coronavirus. Retrieved August 12, 2020, from https://www.cdc.gov/coronavirus/2019-ncov/symptoms-testing/symptoms.html

Chan, K. S., Lai, S. T., Chu, C. M., Tsui, E., Tam, C. Y., Wong, M. M., Tse, M. W., Que, T. L., Peiris, J. S., Sung, J., Wong, V. C., & Yuen, K. Y. (2003). Treatment of severe acute respiratory syndrome with lopinavir/ritonavir: a multicentre retrospective matched cohort study. Hong Kong medical journal = Xianggang yi xue za zhi, 9(6), 399–406.

China Daily. (2003). http://www.chinadaily.com.cn/en/doc/2003-08/31/content_259908.htm

China.org.cn – Xinhua News Agency. (2003). http://english.china.org.cn/english/scitech/73828.htm

Cheung, N., & Mcnab, A. A. (2003). Venous Anatomy of the Orbit. *Investigative Opthalmology & Visual Science*, *44*(3), 988. doi:10.1167/iovs.02-0865

Collell, G., & Fauquet, J. (2015). Brain activity and cognition: A connection from thermodynamics and information theory. *Frontiers in Psychology*, *6*, 818. doi:10.3389/fpsyg.2015.00818

Davis, R. (2020, May 08). IDF vs COVID-19. Retrieved October 21, 2020, from https://ajn.timesofisrael.com/idf-vs-covid-19/

Farnell, S., Maxwell, L., Tan, S., Rhodes, A., & Philips, B. (2005). Temperature measurement: Comparison of non-invasive methods used in adult critical care. *Journal of Clinical Nursing, 14*(5), 632-639. doi:10.1111/j.1365-2702.2004.00916.x

Finnerty, M. (2020, May 29). Brigade Completes Deployment Supporting COVID-19 Response. Retrieved September 12, 2020, from https://www.defense.gov/Explore/Features/Story/Article/2200697/2nd-meb-completes-deployment-supporting-national-covid-19-response/

Festal A. 1887. Recherches anatomiques sur les veines de l'orbite. These de Paris DOI: https://exhibits.lib.unc.edu/exhibits/show/nyam-theses/item/5708.

Forrest, A. J., Juliano, M. L., Conley, S. P., Cronyn, P. D., Mcglynn, A., & Auten, J. D. (2017). Temporal artery and axillary thermometry comparison with rectal thermometry in children presenting to the ED. *The American Journal of Emergency Medicine, 35*(12), 1855-1858. doi:10.1016/j.ajem.2017.06.017

Furukawa, N. W., Brooks, J. T., & Sobel, J. (2020). Evidence Supporting Transmission of Severe Acute Respiratory Syndrome Coronavirus 2 While Presymptomatic or Asymptomatic. *Emerging Infectious Diseases, 26*(7). doi:10.3201/eid2607.201595

Gates, B. (2020). Responding to Covid-19 — A Once-in-a-Century Pandemic? *New England Journal of Medicine, 382*(18), 1677-1679. doi:10.1056/nejmp2003762

Geijer, H., Udumyan, R., Lohse, G., & Nilsagård, Y. (2016). Temperature measurements with a temporal scanner: Systematic review and meta-analysis. *BMJ Open, 6*(3). doi:10.1136/bmjopen-2015-009509

Golovkin, P. (2020, September 11). Russian schools open with classroom, cafeteria precautions. Retrieved October 21, 2020, from https://apnews.com/article/virus-outbreak-archive-russia-a17cd7313045e576392e5ef0858aafce

Hindustan Times. (2020, April 22). Slow restart for Toyota factory amid France's coronavirus lockdown. Retrieved September 14, 2020, from https://auto.hindustantimes.com/auto/news/slow-restart-for-toyota-yaris-factory-amid-france-s-coronavirus-lockdown-41587538355599.html

Ing, A. J., Cocks, C., & Green, J. P. (2020). COVID-19: In the footsteps of Ernest Shackleton. Thorax, 75(8), 693-694. doi:10.1136/thoraxjnl-2020-215091

Jalal, A. (2020, March 04). Coronavirus temperature check. Retrieved September 14, 2020, from https://www.abc.net.au/news/2020-03-04/coronavirus-temperature-check-1/12026250?nw=0

Jensen, B. N., Jensen, F. S., Madsen, S. N., & Løssl, K. (2000). Accuracy of Digital Tympanic, Oral, Axillary, and Rectal Thermometers Compared with Standard Rectal Mercury Thermometers. *The European Journal of Surgery, 166*(11), 848-851. doi:10.1080/110241500447218

Jessen, C., & Kuhnen, G. (1992). No evidence for brain stem cooling during face fanning in humans. *Journal of Applied Physiology, 72*(2), 664-669. doi:10.1152/jappl.1992.72.2.664

Johnson, N. P., & Mueller, J. (2002). Updating the Accounts: Global Mortality of the 1918-1920 "Spanish" Influenza Pandemic. *Bulletin of the History of Medicine, 76*(1), 105-115. doi:10.1353/bhm.2002.0022

Kiekkas, P., Aretha, D., Almpani, E., & Stefanopoulos, N. (2019). Temporal Artery Thermometry in Pediatric Patients: Systematic Review and Meta-Analysis. *Journal of Pediatric Nursing, 46*, 89-99. doi:10.1016/j.pedn.2019.03.004

Kiekkas, P., Stefanopoulos, N., Bakalis, N., Kefaliakos, A., & Karanikolas, M. (2016). Agreement of infrared temporal artery thermometry with other thermometry methods in adults: Systematic review. *Journal of Clinical Nursing, 25*(7-8), 894-905. doi:10.1111/jocn.13117

Kimberger, O., Cohen, D., Illievich, U., & Lenhardt, R. (2007). Temporal Artery Versus Bladder Thermometry During Perioperative and Intensive Care Unit Monitoring. *Anesthesia & Analgesia, 105*(4), 1042-1047. doi:10.1213/01.ane.0000281927.88935.e0

Kun, Z., & Wenting, Z. (2020, March 12). Young adults most stressed by virus. Retrieved September 14, 2020, from https://www.chinadaily.com.cn/a/202003/12/WS5e69730fa31012821727e50f.html

Lagakos, N., & Bucaro, J. A. (2012). *U.S. Patent No. 8195013*. Washington, DC: U.S. Patent and Trademark Office.

Latman, N. S., Hans, P., Nicholson, L., DeLee Zint, S., Lewis, K., Shirey, A. (2001). Evaluation of clinical thermometers for accuracy and reliability. *Biomed Instrum Technol,* 35(4), 259-265.

Lewis, W. C. (1968). *Thermal insulation from wood for buildings: Effects of moisture and its control* (USA, U.S.D.A.). Ft. Belvoir, VA: Defense Technical Information Center.

Lum, C. L., Jeyanthi, S., Prepageran, N., Vadivelu, J., & Raman, R. (2009). Antibacterial and antifungal properties of human cerumen. *The Journal of Laryngology & Otology, 123*(4), 375-378. doi:10.1017/s0022215108003307

MacLean, J.D., 1941. Thermal conductivity of wood. Heating, piping & air conditioning 13:380-391. DOI: https://www.fpl.fs.fed.us/documnts/pdf1941/macle41a.pdf

Mariak Z, Lebkowski W, Lysoń T, Lewko J, Piekarski P. (1999). Temperatura mózgu podczas kraniotomii w znieczuleniu ogólnym [Brain temperature during craniotomy in general anesthesia]. *Neurol Neurochir Pol*., 33(6), 1325-1337.

Martin, S. A., & Kline, A. M. (2004). Can There Be a Standard for Temperature Measurement in the Pediatric Intensive Care Unit? *AACN Clinical Issues: Advanced Practice in Acute and Critical Care, 15*(2), 254-266. doi:10.1097/00044067-200404000-00011

McDonnell, P. J., Linthicum, K., & Wilkinson, T. (2020, March 14). Mexico, Latin America gear up for next phase of coronavirus threat. Retrieved September 11, 2020, from https://www.latimes.com/world-nation/story/2020-03-14/mexico-latin-america-gear-up-for-next-phase-of-coronavirus-threat

Microsoft. (2017, June 9). How do you fast-track a biofeedback device to market in less than a year? Retrieved August 12, 2020, from https://customers.microsoft.com/en-us/story/btt

Modell, J. G., Katholi, C. R., Kumaramangalam, S. M., Hudson, E. C., & Graham, D. (1998). Unreliability of the Infrared Tympanic Thermometer in Clinical Practice. *Southern Medical Journal, 91*(7), 649-654. doi:10.1097/00007611-199807000-00008

Mogensen, C. B., Wittenhoff, L., Fruerhøj, G., & Hansen, S. (2018). Forehead or ear temperature measurement cannot replace rectal measurements, except for screening purposes. *BMC Pediatrics, 18*(1). doi:10.1186/s12887-018-0994-1

Moran, D. S., & Mendal, L. (2002). Core Temperature Measurement. *Sports Medicine, 32*(14), 879-885. doi:10.2165/00007256-200232140-00001

Mori, K. (2020, June 23). "Battle of Okinawa" 75th Anniversary Commemoration. Retrieved October 21, 2020, from https://www.upi.com/News_Photos/lp/9dcdaf90b290a644c2d40ae42bf56c94/

Moritsugu, K. (2020, March 2). China's crisis wanes as epidemic takes hold in US, elsewhere. Retrieved October 22, 2020, from https://apnews.com/article/45393d272612f46899d269b1966c869a

Myers, M. (2020, July 30). The military is seeing a higher COVID-19 infection rate in young people. Here's why. Retrieved October 21, 2020, from https://www.militarytimes.com/news/your-military/2020/07/30/the-military-is-seeing-a-higher-covid-19-infection-rate-in-young-people-officials-explain-why/

Newman, M., Kirchner, J., & Phillips-Bute, B. (2001). Longitudinal assessment of neurocognitive function after coronary-artery bypass surgery. *ACC Current Journal Review, 10*(4), 81-82. doi:10.1016/s1062-1458(01)00339-7

Nordling, L. (2020, March 15). 'A ticking time bomb': Scientists worry about coronavirus spread in Africa. Retrieved August 12, 2020, from https://www.sciencemag.org/news/2020/03/ticking-time-bomb-scientists-worry-about-coronavirus-spread-africa

Normile, D. (2020, March 10). Why airport screening won't stop the spread of coronavirus. Retrieved August 12, 2020, from https://www.sciencemag.org/news/2020/03/why-airport-screening-wont-stop-spread-coronavirus

Niven, D. J., Gaudet, J. E., Laupland, K. B., Mrklas, K. J., Roberts, D. J., & Stelfox, H. T. (2015). Accuracy of Peripheral Thermometers for Estimating Temperature. *Annals of Internal Medicine, 163*(10), 768. doi:10.7326/m15-1150

O'Brien, D. L., Rogers, I. R., Holden, W., Jacobs, I., Mellett, S., Wall, E. J., & Davies, D. (2000). The Accuracy of Oral Predictive and Infrared Emission Detection Tympanic Thermometers in an Emergency Department Setting. *Academic Emergency Medicine, 7*(9), 1061-1064. doi:10.1111/j.1553-2712.2000.tb02101.x

O'Grady, N. P., Barie, P. S., Bartlett, J. G., Bleck, T., Carroll, K., Kalil, A. C., . . . Masur, H. (2008). Guidelines for evaluation of new fever in critically ill adult patients: 2008 update from the American College of Critical Care Medicine and the Infectious Diseases Society of America. *Critical Care Medicine, 36*(4), 1330-1349. doi:10.1097/ccm.0b013e318169eda9

Oxford, J., Lambkin, R., Sefton, A., Daniels, R., Elliot, A., Brown, R., & Gill, D. (2005). A hypothesis: The conjunction of soldiers, gas, pigs, ducks, geese and horses in Northern France during the Great War provided the conditions for the emergence of the "Spanish" influenza pandemic of 1918–1919. Vaccine, 23(7), 940-945. doi:10.1016/j.vaccine.2004.06.035

Oxford, J., Sefton, A., Jackson, R., Innes, W., Daniels, R., & Johnson, N. (2002). World War I may have allowed the emergence of "Spanish" influenza. The Lancet Infectious Diseases, 2(2), 111-114. doi:10.1016/s1473-3099(02)00185-8

Patel, N., Smith, C. E., Pinchak, A. C., & Hagen, J. F. (1996). Comparison of esophageal, tympanic, and forehead skin temperatures in adult patients. *Journal of Clinical Anesthesia, 8*(6), 462-468. doi:10.1016/0952-8180(96)00103-1

Petersdorf, R. G., & Beeson, P. B. (1961). Fever Of Unexplained Origin: Report On 100 Cases. *Medicine, 40*(1), 1-30. doi:10.1097/00005792-196102000-00001

Positively Osceola. (2020, July 15). Epcot and Hollywood Studios to reopen today amid the continued surge of COVID-19 cases in Central Florida. Retrieved September 14, 2020, from https://www.positivelyosceola.com/epcot-and-hollywood-studios-to-reopen-today-amid-the-continued-surge-of-covid-19-cases-in-central-florida/

Priest, P. C., Duncan, A. R., Jennings, L. C., & Baker, M. G. (2011). Thermal Image Scanning for Influenza Border Screening: Results of an Airport Screening Study. *PLoS ONE, 6*(1). doi:10.1371/journal.pone.0014490

Protsiv, M., Ley, C., Lankester, J., Hastie, T., & Parsonnet, J. (2020). Decreasing human body temperature in the United States since the Industrial Revolution. *ELife*, *9*. doi:10.7554/elife.49555

Quatrara, B., Coffman, J., Jenkins, T., Mann, K., McGough, K., Conaway, M., & Burns, S. (2007). The effect of respiratory rate and ingestion of hot and cold beverages on the accuracy of oral temperatures measured by electronic thermometers. Medsurg nursing : official journal of the Academy of Medical-Surgical Nurses, 16(2), 105–100.

Reuters. (2020, May 22). Russia reports record daily rise in new coronavirus deaths. Retrieved September 14, 2020, from https://www.reuters.com/article/health-coronavirus-russia-cases/russia-reports-record-daily-rise-in-new-coronavirus-deaths-idINKBN22Y0WB

Risch, H. A. (2020). Opinion: Early Outpatient Treatment of Symptomatic, High-Risk Covid-19 Patients that Should be Ramped-Up Immediately as Key to the Pandemic Crisis. *American Journal of Epidemiology*. doi:10.1093/aje/kwaa093

Robinson, J. L. (2004). Body temperature measurement in paediatrics: Which gadget should we believe? *Paediatrics & Child Health*, *9*(7), 457-459. doi:10.1093/pch/9.7.457

Sappenfield, J. W., Hong, C. M., & Galvagno, S. M. (2013). Perioperative temperature measurement and management: Moving beyond the Surgical Care Improvement Project. *Journal of Anesthesiology and Clinical Science*, *2*(1), 8. doi:10.7243/2049-9752-2-8

Scripture, E. (1892). The Need of Psychological Training. *Science*, *19*(474), 127-128. Retrieved September 14, 2020, from http://www.jstor.org/stable/1766918

Seery, L. S., Zaldívar, R. A., & Garrity, J. A. (2009). Amaurosis and Optic Disc Blanching During Upgaze in Graves Ophthalmopathy. *Journal of Neuro-Ophthalmology*, *29*(3), 219-222. doi:10.1097/wno.0b013e3181b2842b

Shams, S. (2020, March 18). Coronavirus: Is Pakistan taking COVID-19 too lightly?: DW: 18.03.2020. Retrieved September 14, 2020, from https://www.dw.com/en/coronavirus-is-pakistan-taking-covid-19-too-lightly/a-52824403

Silverman, D. G., Brousseau, D. A., & Engelman, K. (1987). Fluorometric documentation of increased cutaneous blood flow after topical application of a PGE2 analog in man. *Prostaglandins*, *33*(5), 627-638. doi:10.1016/0090-6980(87)90030-x

Suleman, M., Doufas, A. G., Akça, O., Ducharme, M., & Sessler, D. I. (2002). Insufficiency in a New Temporal-Artery Thermometer for Adult and Pediatric Patients. *Anesthesia & Analgesia*, *95*(1), 67-71. doi:10.1097/00000539-200207000-00012

Soo, Y., Cheng, Y., Wong, R., Hui, D., Lee, C., Tsang, K., . . . Sung, J. (2004). Retrospective comparison of convalescent plasma with continuing high-dose methylprednisolone treatment in SARS patients. *Clinical Microbiology and Infection*, *10*(7), 676-678. doi:10.1111/j.1469-0691.2004.00956.x

Sun, H., Xiao, Y., Liu, J., Wang, D., Li, F., Wang, C., . . . Liu, J. (2020). Prevalent Eurasian avian-like H1N1 swine influenza virus with 2009 pandemic viral genes facilitating human infection. *Proceedings of the National Academy of Sciences*, *117*(29), 17204-17210. doi:10.1073/pnas.1921186117

Tandberg, D., & Sklar, D. (1983). Effect of Tachypnea on the Estimation of Body Temperature by an Oral Thermometer. *New England Journal of Medicine*, *308*(16), 945-946. doi:10.1056/nejm198304213081607

Teller, J., Ragazzi, M., Simonetti, G., & Lava, S. (2013). Accuracy of tympanic and forehead thermometers in private paediatric practice. *Acta Paediatrica*, *103*(2). doi:10.1111/apa.12464

TenWolde, A., Mcnatt, J. D., & Krahn, L. (1988). Thermal properties of wood and wood panel products for use in buildings. doi:10.2172/6059532

Today Online. (2020, February 16). 'Thermometer guns' on Covid-19 front lines are 'notoriously not accurate'. Retrieved September 13, 2020, from https://www.todayonline.com/world/thermometer-guns-covid-19-front-lines-are-notoriously-not-accurate

Tomes, N. (2010). "Destroyer and Teacher": Managing the Masses during the 1918–1919 Influenza Pandemic. *Public Health Reports, 125*, 48-62. doi:10.1177/00333549101250s308

Varney, S. M., Manthey, D. E., Culpepper, V. E., & Creedon, J. F. (2002). A comparison of oral, tympanic, and rectal temperature measurement in the elderly. *The Journal of Emergency Medicine, 22*(2), 153-157. doi:10.1016/s0736-4679(01)00457-7

Vastag, B. (2003). Old Drugs for a New Bug. *Jama, 290*(13), 1695. doi:10.1001/jama.290.13.1695

VOA News. (2020, July 11). Pandemic Worsens in US. Retrieved September 12, 2020, from https://www.voanews.com/covid-19-pandemic/pandemic-worsens-us

Wenger, C. B. (2002). Chapter 2: Human Adaptation to Hot Environments. In Textbooks of Military Medicine, *Medical Aspects of Harsh Environments* (Vol. 1, pp. 53-55). Dist. of Columbia, DC: Borden Institute, United States Army Medical Department, AMEDD Center & School. doi:https://www.cs.amedd.army.mil/borden/bookDetail.aspx?ID=eebb9338-2027-46d5-a5f2-f245e2019b6c&pageTitle=Medical%20Aspects%20of%20Harsh%20Environments,%20Vol%201

Yale University. (2003, July 2). Yale Researcher Discovers "Brain Temperature Tunnel" That For The First Time Allows External Continuous Measurement of Brain Temperature. Retrieved August 18, 2020, from https://news.yale.edu/2003/07/02/yale-researcher-discovers-brain-temperature-tunnel-first-time-allows-external-continuou-0

Supplemental Information

MOVIE LEGENDS

Supplemental Movies 1-3 (Real Time Facial Thermal Emission): Movies show infrared (IR) light emission via BTT of resting volunteer (bright red pulsating pixels) sitting in neutral environment. BTT area, represented by red isotherm, has highest intensity of light emission on the face. All other areas lack emission comparable to BTT. Instead, the remainder of the face is characterized by low and variable light emission, represented by gray scale (white to black, representing decreasing emission intensity), but no bright red bright light, as seen at BTT site, is observed elsewhere on the face. Ear canal and forehead have low thermal emission (meaning low temperature), as compared to higher temperature at the BTT site. Bright white halo around BTT, representing the second highest temperature, can be observed.

Movie 1: Subject moved from right to left to expose left BTT and expose left forehead and ears. At all times, BTT is the only area with high emission (bright red pixels); halo, representing the second highest thermal emission, is seen around BTT. **Movie 2:** Infrared light emission from the right side of the face, with focus on the ear and on the medial forehead over the superficial temporal artery. Lighter area (in linear shape) in right forehead indicates the region of right superficial temporal artery, however, despite its large caliber (Figure 1C), the superficial temporal artery shows low emission relative to emission at $SMOS_{BTT}$. No other area, including the ears, has high infrared light emission. Second brightest (white) area is the halo. Superior palpebral region is seen as a small linear whitish streak on the eyelid**. Movie 3:** As the subject turns from left to right, emission is detected initially from the left BTT and then from the right BTT (when the BTT region is in line with the infrared thermal detector). The BTT is seen as a pulsing bright red pixels, and there is no other comparable emission from other facial regions.